Participation of the stress-responsive CDSP32 thioredoxin in the modulation of chloroplast ATP-synthase activity in Solanum tuberosum

Pascal Rey, Patricia Henri, Jean Alric, Laurence Blanchard, Stefania Viola

Participation of the stress-responsive CDSP32 thioredoxin in the modulation of chloroplast ATP-synthase activity in *Solanum tuberosum*

Pascal Rey[1,*], **Patricia Henri**[1], **Jean Alric**[1], **Laurence Blanchard**[2], **Stefania Viola**[1,*]

[1] Aix Marseille Univ, CEA, CNRS, BIAM, Photosynthesis & Environment (P&E) Team, Saint Paul-Lez-Durance, F-13115, France
[2] Aix Marseille Univ, CEA, CNRS, BIAM, Molecular and Environmental Microbiology (MEM) Team, Saint Paul-Lez-Durance, F-13115, France

* Corresponding authors

Author for contact:

Stefania Viola

Photosynthesis & Environment (P&E) Team, Bâtiment 1900, BIAM, CEA Cadarache, Saint-Paul-lez-Durance, F-13115, France

Phone: +33 0782731926

Email: stefania.viola@cea.fr

Keywords: ATP-synthase, saline-alkaline stress, photosynthesis, redox regulation, *Solanum tuberosum*, structure modeling, thioredoxin.

Abstract

Plant thioredoxins (TRXs) are involved in numerous metabolic and signalling pathways, such as light-dependent regulation of photosynthesis. The atypical TRX CDSP32, chloroplastic drought-induced stress protein of 32 kDa, includes two TRX-fold domains and participates in responses to oxidative stress as an electron donor to other thiol reductases. Here, we further characterized potato lines modified for *CDSP32* expression to clarify the physiological roles of the TRX. Upon high salt treatments, modified lines displayed changes in the abundance and redox status of CDSP32 antioxidant partners, and exhibited sensitivity to combined saline-alkaline stress. In non-stressed plants overexpressing CDSP32, a lower abundance of photosystem II subunits and ATP-synthase γ subunit was noticed. The CDSP32 co-suppressed line showed altered chlorophyll *a* fluorescence induction and impaired regulation of the transthylakoid membrane potential during dark/light and light/dark transitions. These data, in agreement with the previously reported interaction between CDSP32 and ATP-synthase γ subunit, suggest that CDSP32 affects the redox regulation of ATP-synthase activity. Consistently, modeling of protein complex 3-D structure indicates that CDSP32 could constitute a suitable partner of ATP-synthase γ subunit. We discuss the roles of the TRX in the regulation of both photosynthetic activity and enzymatic antioxidant network in relation with environmental conditions.

Introduction

Redox post-translational modifications (PTM) in proteins lead to switches modifying enzymatic activity, protein conformation or subcellular distribution. In the presence of reactive oxygen species (ROS), cysteine (Cys) can be oxidized to various forms such as sulfenic acid or disulfide bond, while methionine (Met) can be oxidized to Met sulfoxide (Davies, 2005; Delaunay et al. 2002; Tada et al. 2008). Of note, most redox PTMs in Cys and Met are reversible thanks to the action of thiol reductases (TRs), in which thiol deprotonation of a catalytic cysteine generates a nucleophilic reactive thiolate form. By modulating Cys redox status in interacting partners, TRs play key roles in cell redox homeostasis maintenance and ROS-related signalling transduction pathways (Lu and Holmgren, 2014).

Plant TRs form complex multigene families including thioredoxins (TRXs) (Meyer et al, 2012; Geigenberger et al. 2017) and glutaredoxins (GRXs), which are closely related to TRXs and use glutathione (GSH) as an electron donor (Rouhier et al. 2008). TRXs are ubiquitous small disulfide reductases carrying a two-Cys active site, generally WCGPC. Cytosolic TRXs get reducing power from NADPH-TRX reductases and are involved in various processes such as mobilization of seed reserves upon germination or biotic stress responses (Sweat and Wolpert, 2007; Hägglund et al. 2016). Plastidial TRX isoforms are mainly supplied with electrons from the photosystem I (PSI)/ferredoxin/ferredoxin-TRX-reductase (FTR) pathway and play, in concert with the NADPH-dependent TRX reductase system termed NTRC, essential roles in the regulation of photosynthetic metabolism notably upon dark/light and light/dark transitions (Serrato et al. 2004; Schürmann and Buchanan, 2008; Courteille et al, 2013; Nikkanen et al. 2016; Yoshida et al. 2018; Lampl et al. 2022). Thiol peroxidases such as peroxiredoxins

(PRXs) also fulfil signalling roles via the control of peroxide concentration or direct thiol oxidation in protein partners (Rhee and Woo, 2011; Cerveau et al. 2016a; Liebthal et al. 2018). Other TRX targets like methionine sulfoxide (MetO) reductases (MSRs) maintain protein redox status thanks to redox-active cysteines that reduce peptide-bound MetO (Tarrago et al. 2009; Laugier et al. 2010). By modifying the Cys redox status in a large set of partners (Montrichard et al. 2009), plant TRXs participate in multiple metabolic, developmental and stress-related processes (Gelhaye et al. 2005; Vieira Dos Santos and Rey, 2006; Geigenberger et al. 2017; Montillet et al. 2021).

In addition to canonical TRXs, such as cytosolic h, mitochondrial o and plastidial f, m, x, y and z isoforms, which contain only one TRX-fold domain and a typical active site WCGPC, plants harbour TRXs carrying atypical active site motifs or including other domains (Meyer et al. 2012). Among them, the CDSP32 (Chloroplastic Drought-induced Stress Protein of 32 kDa) TRX, initially identified in potato plants subjected to water deficit (Rey et al. 1998), is induced by various environmental constraints (Pruvot et al. 1996 ; Rey et al. 1998 ; Broin et al. 2000). The protein is composed of two TRX-fold domains with the N-terminal one having no redox-active motif, but instead a SXXS motif, and the C-terminal one displaying an atypical redox-active HCGPC motif (Rey et al. 1998). The involvement of CDSP32 in responses to oxidative stress was established based on the phenotype of transgenic lines (Broin et al. 2002; 2003) and on its capacity to reduce various PRXs and MSRs (Rey et al. 2005; Vieira Dos Santos et al. 2007; Tarrago et al. 2010). Accordingly, ectopic expression of mulberry and cotton *CDSP32* genes in Arabidopsis was found to trigger recovery following a drought period (Sun et al. 2020) and to confer tolerance to osmotic or oxidative stresses (Elasad et al. 2020).

Besides this role in stress response, CDSP32 could function in photosynthesis regulation, because in CDSP32-overexpressing tobacco, Zhang et al. (2020) noticed higher chlorophyll (Chl) content together with a reduced Chl *a*/*b* ratio, and better maintenance of photosynthetic activity upon Cd treatment, compared to wild-type (WT). They hypothesized that the TRX regulates photosynthetic cyclic electron flow and energy dissipation allowing photoprotection upon stress (Zhang et al. 2021). Most importantly, by performing redox proteomics during a dark/light transition in tobacco, Zimmer et al. (2021) revealed that the redox status of both TRX f and CDSP32 is dependent on the rate of linear electron flow, and proposed that the two TRXs act in concert in the regulation of Calvin-Benson cycle activity.

Here, we further characterized potato lines modified for *CDSP32* expression to better delineate the physiological roles of the TRX. We investigated the sensitivity of the modified lines to osmotic and alkaline stress, as well as the effects of such stresses on the abundance and redox status of CDSP32 partners and on the abundance of photosynthetic proteins. We also investigated the effects of modified *CDSP32* expression on photosynthetic metabolism, and in particular on the chloroplast ATP-synthase activity, during dark/light and light/dark transitions. Based on the obtained results, we discuss the role of CDSP32 in photosynthesis regulation in relation with its participation in the maintenance of plastidial redox homeostasis.

Materials and methods

Plant material and growth conditions

Potato (*Solanum tuberosum* L. cv Désirée) lines were propagated *in vitro* on Murashige and Skoog medium, and transferred for growth *in vivo* in a phytotron under LED light (VEGELED Horticulture Floodlights Apollo LL300, Colasse SA, Belgium) (PPFD of 185 µmol.m^{-2}.s^{-1}, 12 h day/12 h night, 23/19°C) in the "Phytotec" platform (CEA, DRF, BIAM). In addition to WT, four transgenic lines co-suppressed for the expression of the potato *CDSP32* gene (termed D4), overexpressing it (D10) or overexpressing in the WT background a mutated form of the TRX, where the catalytic Cys is replaced by a Ser (DM19 and DM15), were used (Broin et al. 2002; Rey et al. 2005). Following transfer on soil, control plants were watered with water the first three days, and then with nutritive solution (Coic and Lesaint, 1971). For salt treatments, the nutritive solution was supplemented with 0.125 M NaCl or 0.1 M $NaHCO_3$. The treatments were applied for 21 days. At this stage, plant height was measured and aerial parts weighed, and samples for chlorophyll determination and protein analyses collected.

Protein extraction and content determination

Pieces from the terminal leaflet of young expanded leaves were blended in liquid N_2, and the powder was resuspended in 50 mM Tris-HCl, pH 8.0, 1 mM phenylmethylsulfonyl fluoride, and 50 mM β-mercaptoethanol. Following centrifugation (14,000 g, 4°C, 20 min), soluble proteins were recovered by precipitation of the supernatant using two acetone volumes and stored at -20°C. The pellet, containing thylakoids, was resuspended in 50 mM Tris-HCl pH 8.0, 1% SDS, agitated for 2 h at 4°C, then centrifuged (14,000 *g*, 4°C, 20 min). Membrane proteins were precipitated at -20°C by the addition of four volumes of acetone to the supernatant. Protein concentration was quantified using the "Protein Quantification BCA Assay" kit (Pierce BCA Protein Assay Kit, Thermo Fisher Scientific).

Western blot analysis

Proteins were separated by SDS-PAGE generally in 13%, or when needed in 8, 10, 11 or 15%, acrylamide gels (Laemmli, 1970) in reducing conditions (0.1 M DTT in solubilization buffer) and electroblotted onto 0.45 µM nitrocellulose (Pall Gelman Sciences). Membranes were stained with Ponceau red to ensure homogenous and proper transfer. The list of primary antibodies raised in rabbit used in this work is presented in Table S1. Membranes could be subsequently subjected to two distinct revelation procedures. In the first procedure, bound antibodies were detected using a goat anti-rabbit secondary antibody coupled to a fluorescent molecule (Alexa Fluor 680, Invitrogen) diluted 1:10,000 using the "Odyssey Infrared Imager" at 680 nm (Licor, Lincoln, NE, USA). Quantification of band intensity was performed using the software associated with the imager. Then the membrane was incubated with another primary serum and revealed using an anti-rabbit immunoglobulin G coupled to alkaline phosphatase (Sigma). Data were acquired from three or four independent experiments and

representative immunoblots are shown. Quantification of band intensities were obtained from biological replicates yielding consistent results.

Chlorophyll content determination

Leaf disks of 0.6 cm diameter were collected on terminal leaflets of young expanded leaves, stored at –80°C before blending in 80% acetone. Following shaking, overnight storage in the dark at 4°C and centrifugation (14,000 g, 20 min), the content in chlorophylls *a* and *b* was measured by spectrophotometry at 647 and 663 nm, and calculated according to Lichtenthaler (1987).

Fluorescence measurements

Chlorophyll fluorescence was measured on leaf fragments using a laboratory-built fluorescence camera. Leaf fragments were harvested from plants incubated in darkness overnight (>12h), and kept on wet Whatman paper in darkness until measurements were performed. Each biological replicate consisted in one leaf fragment harvested from a different plant. Maximal PSII quantum yield [Fv/Fm = (Fm–Fo)/Fm] was measured applying a multi-turnover saturating light pulse (200 ms, 3,000 µmol photons m^{-2} s^{-1}) to dark-adapted leaves. Fluorescence induction curves were measured during 4 minutes of actinic light at the indicated intensities, and Fm' levels after multi-turnover saturating pulses applied during the actinic illumination. PSII quantum yield [Φ_{PSII} = (Fm'-F)/Fm'] was calculated with F and Fm' values measured, respectively, right before and after the first and last saturating pulses of the sequence. Non-Photochemical Quenching (NPQ) was calculated as (Fm-Fm')/Fm'. Actinic light and saturating pulses were provided by orange-red LEDs, measuring pulses (740 µs) by blue LEDs.

ElectroChromic Shift (ECS) measurements

ECS measurements were performed with a laboratory-built Joliot-Type Spectrophotometer (JTS). Short (15 µs) measuring pulses were provided by a sun-like LED (COB V6HD THRIVE WHT SQ 6500K, Bridgelux) filtered via a 520 nm interference filter (Edmund Optics, 10 nm FWHM). Actinic light was provided by orange-red LEDs. Single-turnover saturating flashes (700 nm, duration 6 ns) were provided by a pulsed Nd:YAG laser pumping an optical parametric oscillator (Surelite II, Continuum). For sub-saturating flashes, the laser light was attenuated using a metal grid. Measurements were performed on intact leaves detached right before measuring from plants incubated in darkness overnight (>12h). Each biological replicate consisted in one leaf detached from a different plant.

Electron Transport Rate (ETR) measurements. Dark-adapted leaves were illuminated with the indicated intensities of actinic light for 4 minutes. The photosystem II+photosystem I (PSII+PSI) antenna size and total steady-state ETR were calculated from the slopes of the ECS increase and decay at the onset and offset of the actinic illumination, respectively (for details see Mathiot and Alric, 2021). The absorption changes induced by a single-turnover saturating flash, inducing one charge separation per photosystem (PSII+PSI) were used for normalisation.

Redox-dependent regulation of the ATP-synthase activity.

Activation: absorption changes induced by one sub-saturating flash were recorded in dark-adapted leaves and 2 minutes after a train of n sub-saturating pre-flashes fired at 20 Hz, with n = 20, 50, 100, 200 and 300. For each leaf, the loss in amplitude of the slow ECS decay phase induced by n pre-flashes ($-A_n$) was calculated with respect to the amplitude of the slow ECS decay phase in the dark-adapted leaf (A_{Dark}), setting the amplitude of the slow phase after 300 pre-flashes as the zero value. The number of charge separations per PSII+PSI induced by n pre-flashes was calculated by multiplying n for the ratio between the absorption changes induced by a sub-saturating and a saturating flash.

De-activation in darkness: absorption changes induced by one sub-saturating single-turnover flash were recorded in dark-adapted leaves and at different times t after a train of 300 sub-saturating pre-flashes fired at 20 Hz, with t = 2, 4, 6, 8, 10, 15 and 20 minutes. For each leaf, the recovery in amplitude of the slow ECS decay phase at a time t after the 300 pre-flashes (A_t) was calculated with respect to the amplitude of the slow ECS decay phase in the dark-adapted leaf (A_{Dark}), setting the amplitude of the slow phase at t = 2 min as the zero value.

For each curve, the $-A_n/A_{Dark}$ (activation measurements) and A_t/A_{Dark} (de-activation measurements) values calculated for the absorption changes measured at 395, 595, 789 and 985 ms after the flash were averaged.

Sequence analysis and 3D structure modelling

Sequences of CDSP32 TRXs and related proteins and of ATP-synthase γ subunit among plant, algae and bacteria phyla were found by searching databases and performing BLAST analyses at NCBI: https://blast.ncbi.nlm.nih.gov/Blast.cgi. Prediction of transit peptide was performed at DTU (Technical University of Denmark): https://services.healthtech.dtu.dk/services/TargetP-2.0/. Multiple sequence alignments were carried out using Clustal Omega at EMBL-EBI: https://www.ebi.ac.uk/Tools/msa/clustalo/. Analysis of conserved protein domain family was performed at NCBI: https://www.ncbi.nlm.nih.gov/Structure/cdd/wrpsb.cgi (Wang et al. 2023). The 3D structures of *S. tuberosum* CDSP32 and TRX f were predicted using AlphaFold2 via the software ColabFold (Jumper et al. 2021; Mirdita et al. 2022). The 3D structures of the *S. tuberosum* ATP synthase γ subunit and the complexes between the γ subunit and CDSP32 and TRX f were predicted using a local AlphaFold2 installation (version 2.3.1) (Jumper et al. 2021). All parameters were kept to default values. The quality of each model, presented in supplementary figures, was evaluated using the confidence measures pLDDT (predicted local distance difference test) that indicates the local accuracy, and PAE (predicted aligned error) that assesses the packing between domains or protein chains. Overall confidence in predictions for complexes were based on a combination of all the metrics, including both the predicted template modelling (pTM) score and the interface predicted template modelling (ipTM) score as well as pLDDT and PAE. The 3D structure of *Spinacia oleracea* ATP-synthase and of its γ subunit was obtained from the protein data bank (https://www.rcsb.org, PDB 6FKF). Three-

dimensional structure or model images (rank_1 model for each AlphaFold2 predicted 3D structure) were generated using PyMOL (PyMOL Molecular Graphics System, Version 2.0 Schrödinger, LLC). The 3D modelled structures of proteins or complexes do not include transit peptides, therefore the sequence numbering of all proteins starts after the addressing peptides.

Results

Growth characteristics and chlorophyll content of potato transgenic lines in control conditions

We previously reported the generation of potato lines either lacking the CDSP32 TRX (co-suppressed line D4), or overexpressing the WT protein (line D10) or the Cys-216-Ser active site mutated form in addition to the WT protein (line DM19) (Broin et al. 2002; Rey et al. 2005). In these first assays, we did not notice any obvious growth or development phenotype for these lines in the absence of environmental constraints. As these assays were performed on a limited number of plants and under a different light source (HQI-sodium lamps) than the one used in this work (LED lamps), we first carried out a deeper phenotype characterization in control conditions. WT and transgenic lines displayed similar growth and development features after 3.5 weeks following the transfer from *in vitro* tubes (Fig. 1A). All lines exhibited stem heights in the range of 21 cm and weights of aerial parts close to 30 g (Fig. S1C,D). Based on the somewhat paler leaf colour in plants expressing mutated CDSP32 (DM19), we determined the chlorophyll content of young expanded leaves in the upper crown (Fig. 1C). While WT, co-suppressed (D4) and CDSP32-overexpressing (D10) plants displayed contents between 36 and 38 µg. cm^{-2}, a significantly lower content (less than 33 µg. cm^{-2}) was measured in plants overexpressing the mutated TRX. No difference in the chlorophyll *a*/*b* ratio was observed, indicating that both chlorophyll types were similarly affected in this line (Fig. S1E).

Growth characteristics upon high salt treatments

CDSP32 gene expression is upregulated in WT potato plants upon severe osmotic stress conditions such as drought or exposure to high NaCl concentration (0.3 M) for eight days (Pruvot et al. 1996). Here, we subjected transgenic potato lines to a less deleterious concentration (0.125 M) in watering solution for three weeks. Upon NaCl exposure, the stem height was strongly reduced in all lines (12 cm *vs* 21 cm in control conditions (Figs. 1B, S1A, C). The treatment also led to a dramatic decrease in the weight of aerial parts to *ca*. 17 g (against 30 g in control conditions) in the four potato lines, (Fig. S1D). We noticed that NaCl-treated plants were greener than control ones (Fig. 1B). Consistently, we measured a chlorophyll content higher than 45 µg.cm^{-2} in the same range in all lines (Fig. 1D). This increased level is likely due to the leaf size reduction and thickness increase induced by the NaCl treatment (Fig. 1B), resulting in higher chloroplast density per leaf surface area (Munns and Tester, 2008). Altogether, these data show that the phenotype of potato plants exposed to osmotic stress *via* NaCl treatment at 0.125 M is unaffected by modifications of *CDSP32* expression.

Since some CDSP32 targets like MSRBs are involved in responses to saline-alkaline conditions (Sun et al. 2016) and *CDSP32* expression is down-regulated in such stress conditions (Huihui et al. 2020), we exposed plants to 0.1 M $NaHCO_3$ for three weeks. Similarly to NaCl treatment, watering with $NaHCO_3$ resulted in a strong decrease in plant size for all lines (Fig. 1B and S1B) with a stem height in the range of 12 cm (Fig. S1C). The weight of aerial parts was also strongly reduced upon salt treatment. Interestingly, WT and CDSP32-overexpressing plants exhibited weights of around 15 and 18 g, respectively, while substantially lower values were recorded for the two other lines, particularly for the one overexpressing the mutated form (less than 11 g) where the difference was significant compared to WT (Fig. S1D). Exposure to $NaHCO_3$, in contrast to NaCl, did not affect leaf expansion (Fig 1B). The four potato lines watered with $NaHCO_3$ displayed pale green to yellow leaves, particularly the youngest ones (Fig. S1B). Chlorophyll content measurements revealed that the pigment level decreased in all lines including the WT (15.5 $\mu g.cm^{-2}$), but it was significantly lower in plants overexpressing mutated CDSP32 (*ca.* 9 $\mu g.cm^{-2}$) (Fig. 1E). In this line, as well as in the one overexpressing the non-mutated CDSP32, the chl *a*/*b* ratio was also significantly lower than in WT (Fig. S1E). Taken together, these data show that plants overexpressing inactive CDSP32 are more sensitive than WT to the saline-alkaline stress induced by $NaHCO_3$ exposure.

Abundance of CDSP32 partners and of proteins involved in maintenance of redox homeostasis

We performed Western blot analyses to investigate the abundance of several thiol reductases, most being known to interact with CDSP32. First, we reassessed the abundance of the CDSP32 TRX in the four potato lines grown in control conditions (Fig. 2A). While the protein was not detected in the D4 co-suppressed line, much higher abundances were observed compared to WT in over-expressing lines, with 5- and 8-fold more intense bands in plants expressing WT or mutated forms, D10 and DM19, respectively, as previously reported (Rey et al., 2005). In agreement with previous reports (Pruvot et al. 1996), NaCl treatment led to a noticeable increase in the abundance of the TRX in WT plants. Upon watering with $NaHCO_3$ (Fig. 2A), no change in protein abundance was noticed in WT plants, and decreased amounts were observed in overexpressing lines compared to control conditions.

We then analysed the abundance of known partners of CDSP32, namely PRXs and MSRs. No change in the total abundance of 2-Cys PRX was noticed in control conditions and upon salt treatments depending on *CDSP32* expression level. However, variations were observed regarding the over-oxidized form of the 2-Cys PRX, which is involved in redox signalling (Rey et al. 2007) and detected using specific antibodies (Table S1). In control conditions and compared to WT, this form was less abundant in co-suppressed lines and more abundant in lines overexpressing WT CDSP32, as previously reported (Cerveau et al. 2016b). Interestingly, over-oxidized 2-Cys PRX was also significantly less abundant in plants over-expressing inactive TRX (Fig. 2A, lane 4; Fig. S2A). Almost no difference was noticed in the abundance of over-oxidized PRX among the four genotypes upon NaCl treatment. Upon $NaHCO_3$ exposure, significantly higher amounts of this redox form were revealed in co-suppressed plants and in

plants over-expressing the mutated TRX compared to WT (Fig. 2A, B) in sharp contrast with control conditions. With regard to PRXQ, no noticeable variation was observed in the four lines either in control conditions or upon salt treatments (Fig. 2A). Plastidial NTRC is a main reducer of 2-Cys PRX (Pulido et al. 2010), and involved in response to high salt (Serrato et al. 2004). In control conditions, a band at *ca.* 54 kDa was revealed by the serum raised against Arabidopsis NTRC, with another upper band at *ca.* 56 kDa. The latter could correspond to an oxidized form, clearly detected in non-reducing conditions (Chae et al. 2013). Both forms could be observed in our experiments due to incomplete reduction, as observed for various types of thiol reductases in reducing SDS-PAGE (Cerveau et al., 2016b). Higher amounts of the upper form were noticed upon NaCl treatment in all lines. No substantial change in the abundance of MSRB1, which is efficiently reduced by CDSP32 (Tarrago et al. 2010), was observed depending on potato genotype in control or NaCl conditions (Fig. 2A). In plants watered with $NaHCO_3$, a significantly higher MSRB1 abundance was observed in both co-suppressed (D4) and the overexpression (D10) lines compared to WT (Fig. 2A, B). Finally, we did not observe any substantial variation in MSRA4 amount, except in co-suppressed plants treated with $NaHCO_3$, which showed a significantly higher level compared to other lines (Fig. 2A, B). These data indicate that modifying *CDSP32* expression level substantially affects the redox status of plastidial PRXs and the abundance of MSRs, notably in $NaHCO_3$ salt-stress conditions.

We investigated the abundance of several ROS-scavenging enzymes, since CDSP32 interacts with 2-Cys PRX, a main player in plastidial ROS homeostasis. Stromal, peroxisomal and cytosolic ascorbate peroxidases (APXs) were revealed in potato extracts (Fig. S2B). APXs levels were similar in all genotypes in control conditions, except for somewhat higher levels of peroxisomal and stromal isoforms in D10 plants, and did not change significantly upon NaCl treatment. Of note, watering with $NaHCO_3$ resulted in a strong decrease in the level of cytosolic APX in all lines (Fig. S2B). No significant variation in catalase (CAT) abundance was observed depending on genotype in control and NaCl conditions. In plants watered with $NaHCO_3$, a lower protein level was noticed in the three transgenic lines compared to WT, with the difference being significant in the lines overexpressing the WT and mutated CDSP32 (Fig. S2B, C). In control conditions and upon NaCl treatment, the abundance of plastidial Cu-Zn superoxide dismutase (SOD) was similar in all lines. In plants watered with $NaHCO_3$, we noticed a significantly higher Cu-Zn SOD amount (by more than 40%) in plants over-expressing WT CDSP32 compared to WT (Fig. S2B, C).

Abundance of photosynthetic components and photoprotective proteins

We analysed the abundance of various photosynthetic components, starting with enzymes participating in the Calvin-Benson cycle (CBC), whose activity is redox regulated by TRXs. No genotype-dependent variation in large RuBisCO subunit abundance was observed in plants grown in control conditions or treated with $NaHCO_3$, while somewhat higher levels were observed upon NaCl treatment (Fig. 3A). Phosphoribulokinase (PRK) allows the regeneration of ribulose 1,5-bisphosphate, the CO_2-acceptor

substrate in CBC. No substantial variation was noticed in PRK abundance as a function of growth condition or of genotype (Fig. 3A).

We then investigated the level of several thylakoid proteins involved in light collection, electron transfer, or protective mechanisms. The abundance of major proteins of light-harvesting complexes, LHCB1 and LHCB2, was very similar in the four potato lines in control and salt conditions. In contrast, in comparison with control conditions, the LHCA1 amount was increased upon NaCl watering, and noticeably decreased in plants treated with $NaHCO_3$, particularly those overexpressing mutated CDSP32 (Fig. 3A and S3). Regarding PSII components, we noticed in control conditions a strong decrease (more than 50%) in the abundance of PsbO, one the three subunits of the PSII oxygen-evolving complex located in lumen, in CDSP32 over-expressing plants compared to WT (Fig. 3A lanes 1, 3 and 3B). Further, the protein level was also found to be substantially lower in this line and the one expressing mutated CDSP32 upon $NaHCO_3$ treatment. Most interestingly, similar changes were observed for the D1 protein that together with D2 forms the PSI reaction centre. Indeed, the abundance of D1 was significantly lower in CDSP32 over-expressing plants in control conditions and in plants expressing the mutated TRX upon $NaHCO_3$ exposure (Fig. 3A lanes 1, 3 and 3B).

Zhang et al. (2021) proposed that CDSP32 could regulate photosynthetic cyclic electron transport. Therefore, we investigated the abundance of components of the two cyclic pathways operating around PSI. The protein levels of NDH-H, a subunit of NAD(P)H-like dehydrogenase complex (Rumeau et al. 2007), were strongly reduced protein level in all lines watered with NaCl compared to control and alkaline-saline conditions and no substantial genotype-dependent variation was noticed (Fig. 3). Conversely, the abundance of PGRL1, which has been proposed to be involved in the ferredoxin:plastoquinone reductase cyclic pathway (Hertle et al. 2013), was much higher in plants watered with NaCl, the protein being barely detected in plants grown in control conditions or treated with $NaHCO_3$.

We previously reported that the ATP-synthase γ subunit interacts with CDSP32 in plant extracts overexpressing the mutant TRX form (Rey et al. 2005). In control conditions, we observed a lower amount of this subunit in plants overexpressing the non-mutated TRX than in WT (Fig. 3A lanes 1, 3 and 7B). Salt treatments resulted in an increased abundance of the γ subunit, with a lower level in plants overexpressing CDSP32 compared to WT upon exposure to $NaHCO_3$ (Fig. 3B).

We analysed the abundance of PsbS, a photoprotective protein involved in dissipation of excess energy in conditions of high illumination (Li et al. 2000). We did not observe any significant change in the protein level in relation with CDSP32 expression level, but noticed a slightly higher protein abundance in all lines exposed to NaCl (Fig. 3A). Finally, we examined the abundance of fibrillins (FBN), a family of proteins possessing a lipid-binding motif and presumed among other functions to reduce photooxidative damage to PSII (Yang et al. 2006; Kim and Kim, 2022). We used the serum that we generated against FBN clade1-type in potato, initially named CDSP34 for Chloroplastic-Drought induced Stress Protein of 34 kDa (Pruvot et al. 1996). In control conditions, two FBNs were revealed at

around 34 and 37 kDa, the latter form being more abundant in plants lacking CDSP32 or over-expressing the mutated TRX. Upon NaCl treatment, the FBN1 isoform was much more abundant in the four lines, consistently with our previous results (Pruvot et al. 1996). In contrast, watering with $NaHCO_3$ resulted in a strong decrease of the abundance of the two isoforms in all lines.

PSII function and activity of the electron transport chain

Our biochemical analyses revealed decreased abundance of the PsbO, D1 and ATP-synthese γ subunit in the line overexpressing CDSP32 in the absence of stress (Fig. 3), so we performed several measurements of the photosynthetic activity to investigate the involvement of the TRX in its regulation. We performed fluorescence measurements to assess the effects of altered CDSP32 expression on the maximal PSII quantum yield (Fv/Fm) in dark-adapted leaves and the yield during the transition from darkness to moderate-low light (80 µmol photons m^{-2} s^{-1}, Fig. 4A). Fv/Fm values were similar in all genotypes (~0.79, Fig. 4C and Table S2), indicating a normal PSII function. The transient fluorescence increase in the first seconds of moderate-low illumination was instead significantly higher in the CDSP32 co-suppressed line (D4, Fig. 4B), although it then decreased to similar stationary levels as in the other genotypes during the following 4 minutes of illumination. This resulted in a lower PSII yield (Φ_{PSII}) measured in D4 plants 4 seconds after the light onset (Fig. 4D and Table S2), but a normal Φ_{PSII} *ca.* 200 seconds after the light onset (Fig. 4E and Table S2). We observed an increased transient fluorescence in D4 also during the transition from darkness to moderate-high light (170 µmol photons m^{-2} s^{-1}), although the difference was less pronounced because the increase was generally higher in all genotypes (Fig. S4A, B). In high light (750 µmol photons m^{-2} s^{-1}), the initial fluorescence increase reached values close to Fm in all plants (Fig. S4C, D). The Non Photochemical Quenching (NPQ) of Fm' induced by the medium-high and high lights was similar in all lines (Fig. S4A, C). At all light intensities, the fluorescence rise kinetics in the first hundreds of milliseconds of illumination were similar in all genotypes, suggesting a similar PSII antenna size.

In agreement with the fluorescence results, the PSII+PSI antenna size and total steady-state electron transport rates measured by ElectroChromic Shift (ECS) as a function of light intensity were also similar in all genotypes (Fig. S5).

Light-dependent activation of the ATP-synthase activity

Zimmer et al. (2021) have shown that, during the transition from darkness to low light, the reduction of CDSP32 follows kinetics similar to those of TRX f and of ATP-synthase γ subunit, and here we revealed a lower abundance of this subunit in lines overexpressing CDSP32 in control conditions (Fig. 3). Based on these results and on the interaction between CDSP32 and the γ subunit (Rey et al. 2005), we investigated the redox-dependent activation of ATP-synthase in dark-adapted potato leaves.

The ElectroChromic Shift (ECS) measures the transthylakoid membrane potential (Δψ) generated by the photosynthetic electron and proton transport activity, whose dissipation mostly depends on the ATP-

synthase activity. We thus measured the activity of the ATP-synthase based on the kinetics of ECS decay after a single-turnover flash, inducing charge separation in PSII and PSI, as previously done by Kramer and Crofts (1989). Since high $\Delta\psi$ levels can also induce an increase in ATP-synthase activity (Kramer and Crofts, 1989), we used sub-saturating flashes inducing charge separation in ~55-59% of photosystems in all genotypes (Table S3).

We measured the flash-dependent ECS decay kinetics 2 minutes after different numbers of pre-flashes. After 2 minutes, the $\Delta\psi$ generated by the pre-flashes is dissipated, while the ATP-synthase reduced by the pre-flashes is not yet re-oxidised. In these conditions, an acceleration of the flash-dependent ECS decay thus reflects an increase in the ATP-synthase activity induced by its reduction during the pre-flashes. The ECS decay kinetics were similarly slow in dark-adapted leaves in all genotype, indicating an oxidised and thus inactive ATP-synthase, and fully accelerated after a train of 300 pre-flashes, that induced the reduction-dependent activation of the ATP-synthase. Although the acceleration after 300 pre-flashes was comparable in all genotypes, that for intermediate numbers of pre-flashes was delayed in the co-suppressed D4 line (Fig. 5A). Consequently, the number of charge separations required to achieve a 50% acceleration of the slow ECS decay phase was significantly higher in D4 than in the other genotypes (Fig. 5B, Fig. S6A, B and Table S4). In the DM19 line, expressing a mutated inactive form of CDSP32 in addition to the WT form, we observed a higher degree of variability in the acceleration of the ECS decay kinetics than in the other genotypes. For this reason, we present the results obtained in 5 DM19 biological replicates, instead of 3. Overall, the average number of charge separations required to achieve a 50% acceleration of the slow ECS decay phase in DM19 plants was still significantly lower than in D4 plants (Fig. 5B, Fig. S6B and Table S4).

We then investigated the ATP-synthase de-activation in darkness by measuring the flash-dependent ECS decay kinetics at different times after a train of 300 pre-flashes. While the ECS decay kinetics were equally fast in all genotypes 2 minutes after the pre-flashes, their subsequent deceleration in darkness was faster in the D4 line (Fig. 5C). Consequently, the dark time required to achieve 50% recovery of the slow ECS decay phase was significantly shorter in the D4 line (Fig. 5D, Fig. S6C, D and Table S5).

Together, these results show that the kinetics of ATP-synthase activation and de-activation during dark/light and light/dark transitions are modified in the D4 line, where CDSP32 is absent. The amounts of ATP-synthase γ subunit are close in WT and D4, but significantly lower in the D10 overexpression line (Fig. 3B), where we did not observe changes in kinetics with respect to WT. Therefore, the modified kinetics observed in D4 likely reflect altered redox regulation of the ATP-synthase, that could involve CDSP32 in WT and another TRX with different redox properties in its absence. This hypothesis is in line with the previously identified interaction between CDSP32 and the ATP-synthase γ subunit (Rey et al. 2005), where the regulatory cysteines are present. Both CDSP32 and TRX f have been shown to be reduced with similar kinetics during dark/light transitions (Zimmer et al. 2021), so we made the hypothesis that TRX f could replace CDSP32 in the redox regulation of the ATP-synthase in the D4 line. If this were the case, and assuming that CDSP32 and TRX f are in thermodynamic equilibrium (as

suggested by Zimmer et al. 2021), the data in Fig. 5B and D could be used to calculate an hypothetical equilibrium constant (*K*) between the two TRXs, as detailed in the Supplementary Information. Based on the calculated equilibrium constants (*ca.* 0.3 for the flash-dependent activation data and of *ca.* 0.5 for the dark-dependent de-activation data, Fig. S7), the Em of CDSP32 should be between 16 and 9 mV higher that the Em of the putative substitute TRX, TRX f. This would be in accordance with the published Em values of the two proteins (*ca.* -290 mV for TRX f and -280 mV for CDSP32, as reported in Zimmer et al. 2021).

Thanks to its slightly higher Em, CDSP32 could ensure a fast redox-dependent activation of the ATP-synthase when plants are exposed to low light, and modulate the kinetics of its de-activation in darkness.This could explain the delayed ATP-synthase activation/deactivation phenotype we observed in the D4 co-suppressed line. The transient nature of such phenotype and the poor reactivity of the available antybody with the *S. tuberosum* γ subunit (Fig. S8) have so far prevented us to obtain molecular evidence of a direct redox regulation of the ATP-synthase γ subunit by CDSP32. We therefore used sequence analysis and structure modelling to asses whether CDSP32 could directly modulate activity of the ATP-synthase via its γ subunit.

CDSP32 sequence and structure features

We first investigated whether the CDSP32 sequence features confer specific structural and electrostatic characteristics to the TRX notably compared to canonical plastidial ones such as TRX f. The analysis of CDSP32 sequences in Dicotyledon and Monocotyledon species revealed that the TRX is highly conserved, except the transit peptide, as shown by multiple sequence alignment (Fig. S9). We particularly noticed the presence of a conserved SXXS motif in the N-ter domain at the active site position in the C-ter domain (Rey et al. 1998), and very high identity in the sequence surrounding the active site. This highly conserved sequence constitutes a typical CDSP32 19-residue motif, VLDVGLKHCGPCVKVYPTV, not found in plant canonical TRXs.

The 3D structure of *S. tuberosum* CDSP32 predicted by AlphaFold2 with high confidence shows two TRX-fold domains as expected (TRX_D1 and TRX_D2), each with four α helices surrounding four β strands, separated by a 10-residue flexible region (Fig. 6A, Fig. S10). The AlphaFold2 structure of *S. tuberosum* TRX f shows a single TRX-fold domain that perfectly superimposes on the TRX_D2 domain of CDSP32 including the same position of the redox site motif (H/WCGPC) (Fig. 6A, Fig. S11). Although these TRXs show the same folding, they present different electrostatic properties (Fig. 6B) that can play a crucial role in distinct substrate specificity via electrostatic complementarity with their partners as shown for *Arabidopsis thaliana* TRXs isoforms (Bodnar et al. 2023). Of note, the two TRX-fold domains of CDSP32 (that share 26.8 % identity) also perfectly superimpose but show different electrostatic properties (Fig. 6B, Fig. S10).

Modelling of the CDSP32-ATP-synthase complex

The 3D structure of the complex formed between CDSP32 and the γ subunit of *S. tuberosum* ATP-synthase was modelled using AlphaFold2 to see how these two proteins could interact. Chloroplast ATP-synthase is a macromolecular machine made of 26 protein subunits, 17 of them being embedded in the membrane and the regulatory γ subunit being part of the central stalk as shown in the cryo-EM structure of *Spinacia oleracea* ATP-synthase (Hahn et al. 2018). The AlphaFold2 3D structure of *S. tuberosum* ATP-synthase γ subunit alone shows the same folding as the spinach γ subunit (PDB 6FKF) (83.4 % identity between these two γ-subunits) with two long α-helices in a tight coiled coil that forms the rotor shaft and a L-shaped structure containing the redox loop and a β-hairpin (Fig. 7A, Fig. S12A-B). In the modelled ATP-synthase γ subunit-CDSP32 complex, the γ subunit redox loop and the redox active motif of CDSP32 TRX_D2 are in close proximity with a distance of 4Å between the S of the catalytic Cys of each partner, showing that CDSP32 could reduce the disulphide bridge of the γ subunit redox loop (Fig. 7B, Fig. S13 for all AlphaFold2 confidence metrics). The superposition of the *S. tuberosum* γ subunit-CDSP32 complex on the 3D structure of *S. oleracea* ATP-synthase shows that CDSP32 TRX would have sufficient space to interact with the γ subunit without steric hindrance (Fig 7B). The spinach ATP-synthase γ subunit-CDSP32 complex was also modelled using Afphafold2 and shows the same result (data not shown). It has to be noticed that the L-shaped structure present in the γ subunit alone is no longer structured in the modelled ATP-synthase γ subunit-CDSP32 complex (Fig. 7). These changes are in agreement with the recent proposed model of redox regulation of the ATP-synthase by cooperative function of the redox loop and the β-hairpin (Akiyama et al. 2023).

Modelisation of *S. tuberosum* TRX f in complex with the ATP-synthase γ subunit was also generated using AlphaFold2. In this complex, the redox loop of the γ subunit and the redox active motif of TRX f are not close, with a distance of 30Å between the S of the catalytic Cys of each partner (Fig. S14, all AlphaFold2 confidence metrics in legend). This model suggests that it could be more difficult for TRX f to interact with the γ subunit. Therefore, both redox and structural differences could explain the modified kinetics of ATP-synthase regulation observed in absence of CDSP32, if they depended on TRX f activity.

CDSP32 presence and ATP-synthase redox features in photosynthetic organisms

We then performed an extensive search of databases to investigate the presence of CDSP32 in photosynthetic organisms. We retained proteins displaying only the two very specific features of the TRX, *i.e.* two TRX-fold domains and an atypical active site motif, HCGPC. When extending the search outside Dicotyledons and Monocotyledons (Fig. 8, Figs. S15, S16), we observed that the protein, particularly the typical 19-residue motif, is well-conserved in primitive Angiosperms, one class of Gymnosperms, Pinales, and several classes of Pteridophytes. In Bryophytes, related proteins display sequence divergence in the active site (NCGPC and SCGPC in *P. patens* and *M. polymorpha*, respectively) and in the surrounding sequence (Fig. 8, Fig. S15). The CDSP32 homologous proteins identified in Charophytes, such as *C. braunii*, harbour active sites containing two Cys residues, but no

His preceding the catalytic Cys. In Chlorophytes, very poor conservation of the typical CDSP32 sequence motif was observed, since the potential active site carries only one Cys, for example SAGPC in *C. reinhardtii* (Fig. 8, Fig. S16). Finally, no homologous proteins were identified in Cyanobacteria, indicating a non-prokaryotic origin of the gene, as well as in red Algae, Diatoms and Coccolithophores. Interestingly, the region of the ATP-synthase γ subunit containing the two cysteines that are the targets of redox regulation is also present in plants and green algae, but absent in non-green algae and cyanobacteria (Fig. S17; Akiyama et al. 2023). In conclusion, the CDSP32 TRX is particularly well conserved in vascular plants and the presence of related proteins in Bryophytes and green Algae indicates that this TRX type is specific of the green lineage, like the presence of the redox loop in ATP-synthase γ subunit.

Discussion

Participation of the CDSP32 TRX in salt stress responses

The CDSP32 TRX exhibits very unique features with the presence of two TRX-fold domains in tandem and one atypical HCGPC redox active site. The remarkable conservation of CDSP32 in vascular plants suggests that this atypical TRX fulfils specific physiological functions that cannot be performed as efficiently by other plastidial TRXs, despite their remarkable diversity in higher plants (Meyer et al. 2012). The first data on transgenic potato plants highlighted the participation of CDSP32 in responses to oxidative stress (Broin et al. 2002). We proposed that the TRX fulfils an antioxidant role allowing the maintenance of plastidial redox homeostasis upon environmental constraints. TRXs are recognized as essential components in redox and ROS-related transduction pathways allowing integration of multiple signals generated by climatic constraints (Vieira dos Santos and Rey, 2006; Mittler et al. 2022). This is illustrated by the participation of apoplastic TRX h, mitochondrial TRX o, and plastidial TRXs m in responses to salt or light constraints in rice and Arabidopsis (Zhang et al. 2011; Calderon et al. 2018 ; Serrato et al. 2021). However, while we observed an increased CDSP32 abundance in WT potato leaves upon various NaCl treatments (Fig. 2A; Pruvot et al. 1996), no phenotype was noticed in plants modified in *CDSP32* expression under such a salt exposure (Fig. S1). Potato is classified as a moderately salt-sensitive crop (Hütsch et al. 2018; Chourasia et al. 2021), so the NaCl concentration used here might not be high enough to reveal a CDSP32-dependent response, that we cannot exclude, might occur at higher salt concentrations. Consistently, we observed upon high salinity a decreased CDSP32 level in *Arabidopsis* while its abundance was unaffected in a halophyte related-species (Mrah et al. 2007).

When subjected to 0.1 M $NaHCO_3$, potato plants were much more affected compared to plants watered with 0.125 M NaCl. By comparing the two conditions, we can exclude that the stronger stress phenotype observed upon $NaHCO_3$ treatment is due to sodium toxicity, and attribute it to the fact that $NaHCO_3$, compared to neutral salts, generates also alkaline stress in addition to osmotic stress. Plants overexpressing a mutated form were more susceptible to this treatment as evidenced by growth and chlorophyll content measurements (Fig. 1E, Fig. S1B, D, E). Plant adaptation to saline-alkaline stress

has been only recently investigated (Cao et al. 2022; Rao et al. 2023), and involves common responses with neutral salt stress like accumulation of osmolytes and regulation of ion homeostasis, but also more specific responses to limit pH modification within cells (Cao et al. 2022). Saline-alkaline conditions strongly impair ROS production levels and cell redox homeostasis (Rao et al. 2023). Consistently, we observed that exposure to $NaHCO_3$, unlike to NaCl, results in strongly reduced abundance of cytosolic APX in potato (Fig. S2B). CDSP32 could be involved in a pathway regulating the ROS-scavenging capacity upon alkaline stress since the three lines modified for its expression displayed a reduced CAT abundance. In addition, we noticed a significantly higher abundance of Cu/Zn SOD in the line overexpressing the TRX (Fig. S2C). In other respects, we observed substantial changes in the abundance and/or redox status of CDSP32 partners in saline-alkaline stress conditions. For instance, compared to WT, potato plants lacking the TRX or overexpressing its non-functional form displayed a much higher level of over-oxidized 2-Cys PRX, although overall levels of this protein were unaffected, and the three modified lines exhibited higher abundances of plastidial MSRB1 upon $NaHCO_3$ exposure (Fig. 2). Interestingly, overexpression of 2-Cys PRX was recently reported to confer tolerance to $NaHCO_3$, that was associated to maintained photosynthetic activity and increased ROS scavenging capacity (Wang et al. 2023). In other respects, Sun et al. (2016) revealed interaction of one cytosolic methionine sulfoxide reductase B with a Ca^{2+}-kinase in soybean, leading to activation of ROS-signalling under alkaline stress. Altogether, these findings prompt us to propose that CDSP32 and its PRX and MSR partners, which are involved in signalling pathways (Liebthal et al.2018; Rey and Tarrago 2018), participate in plant responses to saline-alkaline stress, and could help protecting from damage the photosynthetic machinery.

Participation of CDSP32 in photosynthetic metabolism and modulation of ATP-synthase activity

Abundance of components of the photosynthetic apparatus

In comparison with typical TRXs f or m, CDSP32 has been considered to be mainly involved in the maintenance of plastidial redox homeostasis upon stress conditions through interaction with other thiol-reductases such as PRXs and MSRs (Rey et al. 2005). In this work, we provide several lines of evidence showing that the TRX is also involved in the regulation of photosynthetic metabolism at several levels in the absence of stress. Indeed, the DM19 line over-expressing mutated CDSP32 exhibits a reduced chlorophyll content (Fig. 1C), revealing that the presence of a high proportion of inactive CDSP32 affects chlorophyll metabolism and/or biosynthesis. The activity of several enzymes involved in chlorophyll biosynthesis is redox-regulated by various plastidial TRX types including NTRC in relation with 2-Cys PRX (Stenbaek et al. 2008; Da et al. 2017; Richter et al. 2018). The phenotype trait of DM19 could result from irreversible trapping by the mutated TRX of redox-sensitive enzymes involved in chlorophyll metabolism or from the modified redox status of 2-Cys PRX observed in this line (Fig. 2A). In control conditions, the D1 and PsbO subunits of PSII accumulated to significantly lower levels in plants overexpressing CDSP32 than in WT (Fig. 3). Of note, Wang et al. (2013) reported substantially reduced levels of these two PSII subunits in *Arabidopsis* plants lacking three TRX m isoforms, and also

showed redox-based interaction between the D1 subunit and TRXs m. PsbO also interacts with TRX (Montrichard et al. 2009) and thus could be possibly redox-regulated through sensitive cysteines, which would be reduced via a NTRC-dependent pathway providing electrons to this PSII subunit located in the lumen (Ameztoy et al. 2019). A lower abundance of D1 and PsbO subunits could result from impaired expression or increased degradation due to redox modifications, and might be associated with subsequent impairment of PSII function. Nonetheless, the PSII maximum quantum yield (Fv/Fm, Fig. 4C) is normal in the overexpression line, indicating that assembled PSII complexes properly function. From the protein analyses in Fig. 3, we did not observe any difference regarding PSI and PSII light harvesting antennas (LHCA1 and LHCB1/2, respectively) in any of the genotypes grown upon standard conditions. This agrees with the fact that the functional antenna size of PSII measured by fluorescence (Figs. 4B and S4B, D) and of PSII+PSI measured by ECS (Fig. S5B) are similar in all lines. Taken together, these data indicate that PSII function and antenna size are independent on CDSP32 abundance. On the other hand, the fluorescence induction curves show that electron transport downstream of PSII is transiently impaired in the line lacking CDSP32 during dark/light transitions (Fig. 4B, D). This suggests a delay in the early stages of photosynthesis activation. Once the activation is completed, the activity of the electron transport chain is independent of *CDSP32* expression, as indicated by the similar levels of stationary Φ_{PSII} and NPQ (which depends on the lumen acidification induced by electron transport) reached in all genotypes (Fig. 4 and S4). This is further confirmed by the similar steady-state electron transport rates measured by ECS as a function of light intensity (Fig. S5).

Regulation of ATP-synthase activity during dark/light and light/dark transitions

Zimmer et al. (2021) have shown that, during the transition from darkness to low light (40 µmol photons m^{-2} s^{-1}), the reduction of the ATP-synthase γ subunit is completed within the first 30 seconds of illumination, while that of the Calvin-Benson cycle enzymes requires a couple of minutes, in accordance with the kinetics of their light-dependent activation reported in previous works (Laing et al. 1981, Wirtz et al. 1982, Kramer et al. 1990). The reduction of CDSP32 and TRX f also peaks at 30 seconds of illumination. This agrees with the proposal made by Kramer and Crofts (1989) that the ATP-synthase activation, which only requires very low light intensities, depends on the redox equilibrium between the γ subunit and TRXs, and should not be limiting for photosynthesis in normal conditions. In our induction curves in medium-low light (Fig. 4), we can attribute the initial transient increase of fluorescence to an over-reduction of the electron transport chain caused by an inactive CBC. This fluorescence transient is higher in the absence of CDSP32 at few seconds after the light onset, but then decreases with similar kinetics in all genotypes during the first minute of illumination. This suggests a similar activation of Calvin-Benson cycle enzymes in all genotypes, with the fluorescence phenotype in the D4 line being due to an impairment in a process that occurs over a shorter time-scale. Based on the previously detected *ex planta* interaction between CDSP32 and the γ subunit (Rey et al. 2005), we hypothesize this process to be the activation of the ATP-synthase. Our ECS measurements show that the light-dependent

activation of the ATP-synthase still occurs in the absence of CDSP32 (D4 plants), but requires more charge separations in PSII and PSI than in the WT, and therefore a higher reduction level of the stroma (Fig. 5B). Concomitantly, the dark reoxidation of the ATP-synthase after illumination is faster in the absence of CDSP32 (Fig. 5D). When the mutated CDSP32 is expressed in addition to the active form (DM19), the kinetics of ATP-synthase activation remain on average faster than in absence of the TRX, but present a higher degree of variability between biological replicates (Fig. 5B and Fig. S6B), possibly reflecting a variability in the relative accumulation levels of the two CDSP32 forms. Plants overexpressing the WT TRX form did not show any significant difference in the kinetics of ATP-synthase activation and de-activation, although a reduced abundance of γ subunit was observed in this line (Fig. 5 and Fig. 3B). Based on these results, we propose that CDSP32 could be responsible for the early stages of redox activation of the ATP-synthase (via the reduction of its γ subunit) during dark/light transition. Additionally, CDSP32 might delay ATP-synthase reoxidation during light/dark transition, possibly acting as a storage of reducing power due to its high abundance in the chloroplast. In D4 plants lacking CDSP32, this redox regulation could be performed by another thioredoxin, but with delayed kinetics. Zimmer et al. (2021) have shown that TRX f is reduced with very similar kinetics to both CDSP32 and ATP-synthase γ subunit during the initial phases of illumination, so this canonical TRX could fulfil the CDSP32 function in co-suppressed plants. In DM19 plants, the mutated CDSP32 could prevent a fraction of the ATP-synthase to be activated during the dark/light transition, in competition with the WT form or TRX f, by irreversible trapping of the γ subunit.

The ATP-synthase has been identified as one of the first photosynthetic components regulated by the TRX system (Mc Kinney et al. 1978) via the control of the redox status of two Cys residues situated in a 9-residue loop domain of the γ subunit (called the redox loop) (Akiyama et al. 2023). Various plastidial TRX systems depending on NTRC or FTR (via TRXs f and m) have been reported to modulate the activity of the ATP-synthase complex (Yoshida et al. 2022; Diaz et al. 2020; Sekiguchi et al. 2020). Rapid reduction of ATP-synthase γ subunit has been noticed under low-light conditions that do not lead to reduction of CBC enzymes, revealing differential dependency on linear electron transfer between this subunit and enzymes like SBPase or FBPase (Hisabori et al. 2013; Yoshida et al. 2014). Of note, the NTRC system has been proposed to be a key activator of the ATP-synthase under low irradiance conditions (Nikkanen et al. 2016). Our data reveal that plants lacking CDSP32 display delayed activation of ATP-synthase during transition from dark to low light, indicating that, if CDSP32 is indeed responsible for the fast activation step, other plastidial TRXs cannot compensate as efficiently the absence of the TRX. This could arise from specific intrinsic properties of this atypical TRX such as a slightly higher E_m, or the more negative electrostatic surface charge compared to TRX f (Fig. 6B).

Modelisation data suggest that it could be more difficult for TRX f, compared to CDSP32, to interact with the γ subunit. Indeed, in the modelled γ subunit-CDSP32 complex, the interaction zone of CDSP32 is located almost exclusively in TRX_D2 (Fig. S13D) in a region showing different electrostatic properties with those of TRX f (Fig. 6B). Of note, the complex generated by AlphaFold2 between the

γ subunit and CDSP32 TRX-D2 only shows the same position for TRX-D2 as in the complex involving the whole CDSP32 indicating that CDSP32 TRX_D1 might not be crucial for the interaction with the ATP-synthase γ subunit (data not shown). These data raise the question of the role of this N-terminal domain, which is unique to CDSP32. Other large TRXs carry domains with known functions such as protein disulphide isomerase activity or interaction with heat shock proteins (Meyer et al. 2012). Taking into account the beneficial stabilizing properties of the TRX-fold, which are widely used for producing recombinant proteins, TRX-D1 might help stabilizing and/or positioning the CDSP32 TRX within the ATP-synthase complex.

Taken collectively, our previous data revealing that the ATP-synthase γ subunit is an *ex planta* target of CDSP32 (Rey et al. 2005), the impaired light-dependent activation of ATP-synthase activity in potato lines lacking the TRX and the modelisation data of the CDSP32-ATP-synthase complex argue for a physiological function for CDSP32 in redox modulation of ATP-synthase activity in relation with environmental conditions and plastidial redox status. However, molecular evidence of a direct redox regulation of the ATP-synthase γ by CDSP32 is still missing, and further work will be required to fully validate this hypothesis.

Nonetheless, it is interesting to note that both CDSP32 and the region of the ATP-synthase γ subunit containing the two cysteines that are the targets of redox regulation are present in plants and green algae, but absent in Cyanobacteria (Figs. 8, S15; Akiyama et al. 2023). When extending the search for CDSP32 homologues to other eukaryotic lineages, we could not find any in red Algae and in organisms whose chloroplast derives from them, such as diatoms and coccolithophores. Interestingly, the ATP-synthase γ subunit of these organisms also lacks the two cysteines that are the targets of redox regulation in plants and green algae (Fig. 8, Fig. S17). It is tempting to speculate that CDSP32 and the γ subunit redox-active cysteines could have evolved together after the endosymbiotic event, from which the chloroplast originated. Indeed, a redox fine-tuning of the ATP-synthase activity during light transitions makes sense in the chloroplast, where the stroma is relatively isolated from the surrounding cellular environment, and its redox poise closely reflects the photosynthetic electron transport activity. This supports the idea of a possible evolutionary correlation between the presence of CDSP32 and the redox fine-tuning of the ATP-synthase activity, that seems to be specific to the green eukaryotic lineage. In Cyanobacteria, instead, the thylakoid membranes are embedded in the cytoplasm, whose redox poise does not change rapidly in function of the sole photosynthetic electron transport activity. Sugar catabolism reduces the cytosolic NADPH pool also in darkness to sustain the activity of the respiratory electron transport chain (Mi et al. 1994) that is also located in the thylakoids (Mullineaux, 2013). The reducing conditions maintain the ATP-synthase active in darkness (Viola et al. 2019), to produce ATP using the proton motive force generated by respiration. The absence of this fine-tuning in red Algae and derivatives might reflect a closer metabolic interaction between chloroplasts and mitochondria, as characterised in diatoms (Bailleul et al. 2015), that could partially uncouple the redox poise of the stroma from photosynthetic electron transport.

Conclusions

CDSP32 is one of the most highly expressed TRX in photosynthetic cells, and its synthesis is strongly triggered upon stress conditions (Rey et al. 1998; Broin et al. 2000; Belin et al. 2015). This argues for an essential function of CDSP32 in the maintenance of chloroplast redox homeostasis and regulation of photosynthetic activity in relation to environmental conditions. CDSP32 interacts with the 2-Cys PRX, a major plastidial thiol peroxidase acting as a redox sensor of H_2O_2, the concentration of which is increased upon stress conditions (Vogelsang and Dietz, 2020). H_2O_2 reacts with 2-Cys PRXs (Dietz, 2008), which in turn can oxidize TRXs and deactivate photosynthetic enzymes (Yoshida et al. 2018). H_2O_2 would thus fulfil, in addition to an electron sink role, a regulatory function via thiol reductases under stress conditions (Driever and Baker, 2011). In addition to its possible involvement in the regulation of ATP-synthase activity during light/dark and dark/light transitions, CDSP32 could thus modulate the activity of the photosynthetic machinery under stress conditions leading to ROS production. Salt-induced osmotic stress conditions results in increased ATP-synthase abundance particularly upon NaCl treatment (Fig. 3A, B) Interestingly, Kohzuma et al. (2009) reported a substantially reduced abundance of this subunit in watermelon plants subjected to drought. Thus, such stress conditions are likely to result in impaired activity of this complex. Kohzuma et al. (2009) proposed that ATP-synthase represents a key point allowing proper photosynthetic proton circuit during acclimation of plant to long-term environmental constraints. It is tempting to speculate that the higher CDSP32 abundance observed in drought-stressed potato plants (Rey et al. 1998) could help maintaining ATP-synthase activation despite a reduced amount of this complex. In other respects, all potato lines exhibited strongly reduced growth and decreased chlorophyll content when exposed to $NaHCO_3$ (Fig. S1). This could originate from pH alteration within plastidial sub-compartments due to saline-alkaline stress, and subsequent impaired functioning of ATP-synthase. Of note, the line expressing the CDSP32 mutant form was found to be more sensitive than WT to $NaHCO_3$, possibly due to more severe disturbance of the ATP-synthase machinery resulting from irreversible trapping of the γ subunit (Rey et al. 2005).

Funding
This work was funded by a transverse project of the BIAM Institute and by Agence Nationale de la Recherche, Grant Award Number: ANR-23-CE20-0009.

Acknowledgements
We are very grateful to Séverine Boiry and the "Phytotec" platform (CEA, DRF, BIAM) for technical assistance with growth chambers. We thank Dr Eevi Rintamäki (University of Turku, Finland) for providing the serum raised against Arabidopsis NTRC.

References

Akiyama K, Ozawa SI, Takahashi Y, Yoshida K, Suzuki T, Kondo K, Wakabayashi KI, Hisabori T. Two specific domains of the γ subunit of chloroplast FoF1 provide redox regulation of the ATP synthesis through conformational changes. *Proc Natl Acad Sci USA*. 2023:120(6):e2218187120. https://doi.org/10.1073/pnas.2218187120

Ameztoy K, Baslam M, Sánchez-López ÁM, Muñoz FJ, Bahaji A, Almagro G, García-Gómez P, Baroja-Fernández E, De Diego N, Humplík JF, Ugena L, Spíchal L, Doležal K, Kaneko K, Mitsui T, Cejudo FJ, Pozueta-Romero J. Plant responses to fungal volatiles involve global posttranslational thiol redox proteome changes that affect photosynthesis. *Plant Cell Environ*. 2019:42(9):2627-2644. https://doi.org/10.1111/pce.13601

Bailleul B, Berne N, Murik O, Petroutsos D, Prihoda J, Tanaka A, Villanova V, Bligny R, Flori S, Falconet D, Krieger-Liszkay A, Santabarbara S, Rappaport F, Joliot P, Tirichine L, Falkowski PG, Cardol P, Bowler C, Finazzi G. Energetic coupling between plastids and mitochondria drives CO_2 assimilation in diatoms. Nature 2015:524:366–369. https://doi.org/10.1038/nature14599.

Belin C, Bashandy T, Cela J, Delorme-Hinoux V, Riondet C, Reichheld JP. A comprehensive study of thiol reduction gene expression under stress conditions in *Arabidopsis thaliana*. *Plant Cell Environ.* 2015:38(2):299-314. https://doi.org/10.1111/pce.12276

Bodnar Y, Gellert M, Hossain FM, Lillig CH. Breakdown of Arabidopsis thaliana thioredoxins and glutaredoxins based on electrostatic similarity-Leads to common and unique interaction partners and functions. *PLoS One*. 2023:18(9):e0291272. https://doi.org/10.1371/journal.pone.0291272

Broin M, Cuiné S, Eymery F, Rey P. The plastidic 2-cysteine peroxiredoxin is a target for a thioredoxin involved in the protection of the photosynthetic apparatus against oxidative damage. *Plant Cell*. 2002:14(6):1417-1432. https://doi.org/10.1105/tpc.001644

Broin M, Cuiné S, Peltier G, Rey P.Involvement of CDSP 32, a drought-induced thioredoxin, in the response to oxidative stress in potato plants. *FEBS Lett.* 2000:467(2-3):245-248. https://doi.org/10.1016/s0014-5793(00)01165-0

Broin M, Rey P.Potato plants lacking the CDSP32 plastidic thioredoxin exhibit overoxidation of the BAS1 2-cysteine peroxiredoxin and increased lipid peroxidation in thylakoids under photooxidative stress. *Plant Physiol*. 2003:132(3):1335-1343. https://doi.org/10.1104/pp.103.021626

Calderón A., Sánchez-Guerrero A., Ortiz-Espín A., Martínez-Alcalá I., Camejo D., Jiménez A. & Sevilla F. Lack of mitochondrial thioredoxin o1 is compensated by antioxidant components under salinity in *Arabidopsis thaliana* plants. *Physiol Plant*. 2018:164(3): 251-267. https://doi.org/10.1111/ppl.12708

Cao Y, Song H, Zhang L. New insight into plant saline-alkali tolerance mechanisms and application to breeding. *Int J Mol Sci*. 2022:23(24):16048.
https://doi.org/10.3390/ijms232416048

Cerveau D, Kraut A, Stotz HU, Mueller MJ, Couté Y, Rey P. Characterization of the *Arabidopsis thaliana* 2-Cys peroxiredoxin interactome. *Plant Sci.* 2016a:252:30-41.
https://doi.org/10.1016/j.plantsci.2016.07.003

Cerveau D, Ouahrani D, Marok MA, Blanchard L, Rey P. Physiological relevance of plant 2-Cys peroxiredoxin overoxidation level and oligomerization status. *Plant Cell Environ.* 2016b:39(1):103-19.
https://doi.org/10.1111/pce.12596

Chae HB, Moon JC, Shin MR, Chi YH, Jung YJ, Lee SY, Nawkar GM, Jung HS, Hyun JK, Kim WY, Kang CH, Yun DJ, Lee KO, Lee SY. Thioredoxin reductase type C (NTRC) orchestrates enhanced thermotolerance to Arabidopsis by its redox-dependent holdase chaperone function. *Mol Plant*. 2013:6(2):323-336.
https://doi.org/10.1093/mp/sss105

Chourasia KN, Lal MK, Tiwari RK, Dev D, Kardile HB, Patil VU, Kumar A, Vanishree G, Kumar D, Bhardwaj V, Meena JK, Mangal V, Shelake RM, Kim JY, Pramanik D. Salinity stress in potato: Understanding physiological, biochemical and molecular responses. *Life (Basel).* 2021 :11(6):545.
https://doi.org/10.3390/life11060545

Coic Y, Lesaint C. Comment assurer une bonne nutrition en eau et ions minéraux en horticulture. *Horticulture Française*. 1971 :8 :11-14.

Courteille A, Vesa S, Sanz-Barrio R, Cazalé AC, Becuwe-Linka N, Farran I, Havaux M, Rey P, Rumeau D. Thioredoxin m4 controls photosynthetic alternative electron pathways in Arabidopsis. *Plant Physiol.* 2013 :161(1):508-20.
https://doi.org/10.1104/pp.112.207019

Da Q, Wang P, Wang M, Sun T, Jin H, Liu B, Wang J, Grimm B, Wang HB. Thioredoxin and NADPH-dependent thioredoxin reductase C regulation of tetrapyrrole biosynthesis. *Plant Physiol.* 2017:175(2):652-666.
https://doi.org/10.1104/pp.16.01500

Davies MJ. The oxidative environment and protein damage. *Biochim Biophys Acta*. 2005:1703(2):93-109.
https://doi.org/10.1016/j.bbapap.2004.08.007

Delaunay A, Pflieger D, Barrault MB, Vinh J, Toledano MB. A thiol peroxidase is an H_2O_2 receptor and redox-transducer in gene activation. *Cell*. 2002:111(4):471-‘81.
https://doi.org/10.1016/s0092-8674(02)01048-6

Dietz KJ. Redox signal integration: from stimulus to networks and genes. *Physiol Plant*. 2008:133(3):459-‘68.
https://doi.org/10.1111/j.1399-3054.2008.01120.x

Driever SM, Baker NR. The water-water cycle in leaves is not a major alternative electron sink for dissipation of excess excitation energy when CO_2 assimilation is restricted. *Plant Cell Environ*. 2011:34:837-846.
https://doi.org/10.1111/j.1365-3040.2011.02288.x

Elasad M, Ahmad A, Wang H, Ma L, Yu S, Wei H. Overexpression of CDSP32 (GhTRX134) cotton gene enhances drought, salt, and oxidative stress tolerance in Arabidopsis. *Plants (Basel)*. 2020:9(10):1388.
https://doi.org/10.3390/plants9101388

Geigenberger P, Thormählen I, Daloso DM, Fernie AR. The unprecedented versatility of the plant thioredoxin system. *Trends Plant Sci*. 2017:22(3):249-262.
https://doi.org/10.1016/j.tplants.2016.12.008

Gelhaye E, Rouhier N, Navrot N, Jacquot JP. The plant thioredoxin system. *Cell Mol Life Sci*. 2005:62(1):24-35.
https://doi.org/10.1007/s00018-004-4296-4

Guinea Diaz M, Nikkanen L, Himanen K, Toivola J, Rintamäki E. Two chloroplast thioredoxin systems differentially modulate photosynthesis in Arabidopsis depending on light intensity and leaf age. *Plant J*. 2020:104(3):718-734.
https://doi.org/10.1111/tpj.14959

Hägglund P, Finnie C, Yano H, Shahpiri A, Buchanan BB, Henriksen A, Svensson B. Seed thioredoxin h. *Biochim Biophys Acta*. 2016:1864(8):974-882.
https://doi.org/10.1016/j.bbapap.2016.02.014

Hahn A, Vonck J, Mills DJ, Meier T, Kuhlbrandt W. Structure, mechanism, and regulation of the chloroplast ATP synthase. *Science*. 2018:360(6389):eaat4318.
https://doi.org/10.1126/science.aat4318.

Hertle AP, Blunder T, Wunder T, Pesaresi P, Pribil M, Armbruster U, Leister D. PGRL1 is the elusive ferredoxin-plastoquinone reductase in photosynthetic cyclic electron flow. Mol Cell. 2013:49(3):511-23.
https://doi.10.1016/j.molcel.2012.11.030.

Hisabori T, Sunamura E, Kim Y, Konno H. The chloroplast ATP synthase features the characteristic redox regulation machinery. *Antioxid Redox Signal*. 2013:19(15):1846-1854.
https://doi.org/10.1089/ars.2012.5044

Huihui Z, Xin L, Yupeng G, Mabo L, Yue W, Meijun A, Yuehui Z, Guanjun L, Nan X, Guangyu S. Physiological and proteomic responses of reactive oxygen species metabolism and antioxidant machinery in mulberry (*Morus alba* L.) seedling leaves to NaCl and $NaHCO_3$ stress. *Ecotoxicol Environ Saf.* 2020:193:110259.
https://doi.org/10.1016/j.ecoenv.2020.110259

Hütsch BW, Keipp K, Glaser AK, Schubert S. Potato plants (*Solanum tuberosum* L.) are chloride-sensitive: Is this dogma valid? *J Sci Food Agric*. 2018:98(8):3161-3168.
https://doi.org/10.1002/jsfa.8819

Jumper J, Evans R, Pritzel A, Green T, Figurnov M, Ronneberger O, Tunyasuvunakool K, Bates R, Žídek A, Potapenko A, Bridgland A, Meyer C, Kohl SAA, Ballard AJ, Cowie A, Romera-Paredes B, Nikolov S, Jain R, Adler J, Back T, Petersen S, Reiman D, Clancy E, Zielinski M, Steinegger M, Pacholska M, Berghammer T, Bodenstein S, Silver D, Vinyals O, Senior AW, Kavukcuoglu K, Kohli P, Hassabis D. Highly accurate protein structure prediction with AlphaFold. *Nature*. 2021:596(7873):583-589.
https://doi.org/10.1038/s41586-021-03819-2.

Kim I, Kim HU. The mysterious role of fibrillin in plastid metabolism: current advances in understanding. *J Exp Bot.* 2022:73(9):2751-2764.

https://doi.org/10.1093/jxb/erac087

Kohzuma K, Cruz JA, Akashi K, Hoshiyasu S, Munekage YN, Yokota A, Kramer DM. The long-term responses of the photosynthetic proton circuit to drought. *Plant Cell Environ*. 2009:32(3):209-19. https://doi.org/10.1111/j.1365-3040.2008.01912.x.

Kramer D.M., Crofts A.R. Activation of the chloroplast ATPase measured by the electrochromic change in leaves of intact plants. *Biochim Biophys Acta Bioenerg.* 1989:976, 28–41. https://doi.org/10.1016/S0005-2728(89)80186-0

Kramer D.M., Wise R.R., Frederick J.R., Alm D.M., Hesketh J.D., Ort D.R., Crofts A.R., Regulation of coupling factor in field-grown sunflower: A Redox model relating coupling factor activity to the activities of other thioredoxin-dependent chloroplast enzymes, *Photosynth Res*. 1990:26, 213–222. https://doi.org/10.1007/BF00033134.

Laemmli UK. Cleavage of structural proteins during the assembly of the head of bacteriophage T4. *Nature*. 1970:227(5259):680-685. https://doi.org/10.1038/227680a0

Laing W.A., Stitt M., Heldt H.W., Control of CO2 fixation. Changes in the activity of ribulosephosphate kinase and fructose- and sedoheptulose-bisphosphatase in chloroplasts, *Biochim Biophys Acta Bioenerg*. 1981:637,348–359. https://doi.org/10.1016/0005-2728(81)90174-2.

Lampl N, Lev R, Nissan I, Gilad G, Hipsch M, Rosenwasser S. Systematic monitoring of 2-Cys peroxiredoxin-derived redox signals unveiled its role in attenuating carbon assimilation rate. *Proc Natl Acad Sci USA*. 2022:119(23):e2119719119. https://doi.org/10.1073/pnas.2119719119

Laugier E, Tarrago L, Vieira Dos Santos C, Eymery F, Havaux M, Rey P. *Arabidopsis thaliana* plastidial methionine sulfoxide reductases B, MSRBs, account for most leaf peptide MSR activity and are essential for growth under environmental constraints through a role in the preservation of photosystem antennae. *Plant J*. 2010:61(2):271-282. https://doi.org/10.1111/j.1365-313X.2009.04053.x

Li XP, Björkman O, Shih C, Grossman AR, Rosenquist M, Jansson S, Niyogi KK. A pigment-binding protein essential for regulation of photosynthetic light harvesting. *Nature* 2000:403:391–395. https://doi.org/10.1038/35000131

Lichtenthaler HK. Chlorophylls and carotenoids: pigments of photosynthetic biomembranes. *Meth Enzymol* 1987:148,350-382. https://doi.org/10.1016/0076-6879(87)48036-1

Liebthal M, Maynard D, Dietz KJ. Peroxiredoxins and redox signaling in plants. *Antioxid Redox Signal*. 2018:28(7):609-624. https://doi.org/10.1089/ars.2017.7164

Lu, J., Holmgren, A. The Thioredoxin Antioxidant System. *Free Radic Biol Med* 2014:66, 75–87. https://doi.org/10.1016/j.freeradbiomed.2013.07.036.

Mathiot C, Alric J. Standard units for ElectroChromic Shift measurements in plant biology. *J Exp Bot*. 2021:72(18):6467-6473. https://doi.org/10.1093/jxb/erab261.

Mckinney DW, Buchanan BB, Wolosiuk RA. Activation of chloroplast ATPase by reduced thioredoxin. *Phytochemistry* 1978:17, 794–795.
https://doi.org/10.1016/S0031-9422(00)94230-4

Meyer Y, Belin C, Delorme-Hinoux V, Reichheld JP, Riondet C. Thioredoxin and glutaredoxin systems in plants: molecular mechanisms, crosstalks, and functional significance. *Antioxid Redox Signal*. 2012:17(8):1124-1160.
https://doi.org/10.1089/ars.2011.4327

Mi H, Endo T, Schreiber U, Ogawa T, Asada K. NAD(P)H dehydrogenase-dependent cyclic electron flow around photosystem I in the cyanobacterium Synechocystis PCC 6803: a study of dark-starved cells and spheroplasts. *Plant Cell Phys*. 1994:35(2):163–173.
https://doi.org/10.1093/oxfordjournals.pcp.a078580.

Mirdita M, Schütze K, Moriwaki Y, Heo L, Ovchinnikov S, Steinegger M. ColabFold: making protein folding accessible to all. *Nat Methods*. 2022: 19(6): 679–682.
https://doi.org/10.1038/s41592-022-01488-1.

Mittler R, Zandalinas SI, Fichman Y, Van Breusegem F. Reactive oxygen species signalling in plant stress responses. *Nat Rev Mol Cell Biol*. 2022:23(10):663-679.
https://doi.org/10.1038/s41580-022-00499-2

M'rah S, Ouerghi Z, Eymery F, Rey P, Hajji M, Grignon C, Lachaâl M. Efficiency of biochemical protection against toxic effects of accumulated salt differentiates *Thellungiella halophila* from *Arabidopsis thaliana*. *J Plant Physiol*. 2007:164(4):375-384.
https://doi.org/10.1016/j.jplph.2006.07.013

Montillet JL, Rondet D, Brugière S, Henri P, Rumeau D, Reichheld JP, Couté Y, Leonhardt N, Rey P. Plastidial and cytosolic thiol reductases participate in the control of stomatal functioning. *Plant Cell Environ*. 2021:44(5):1417-1435.
https://doi.org/10.1111/pce.14013

Montrichard F, Alkhalfioui F, Yano H, Vensel WH, Hurkman WJ, Buchanan BB. Thioredoxin targets in plants: the first 30 years. *J Proteomics*. 2009:72(3):452-474.
https://doi.org/10.1016/j.jprot.2008.12.002

Mullineaux CW. Co-existence of photosynthetic and respiratory activities in cyanobacterial thylakoid membranes. *Biochim Biophys Acta.* 2014:1837(4):503-11.
https://doi.org/10.1016/j.bbabio.2013.11.017

Munns R, Tester M. Mechanisms of salinity tolerance. *Annu Rev Plant Biol*. 2008:59:651-681.
https://doi.org/10.1146/annurev.arplant.59.032607.092911

Nikkanen L, Toivola J, Rintamäki E. Crosstalk between chloroplast thioredoxin systems in regulation of photosynthesis. *Plant Cell Environ*. 2016:39(8):1691-1705.
https://doi.org/10.1111/pce.12718

Pruvot G, Massimino J, Peltier G, Rey P (1996) Effects of low temperature, high salinity and exogenous ABA on the synthesis of two chloroplastic drought-induced proteins in *Solanum tuberosum. Physiol Plant* 1996:97(1):123-131.
https://doi.org/10.1111/j.1399-3054.1996.tb00488.x

Pulido P., Spınola M.C., Kirchsteiger K., Guinea M., Pascual M.B., Sahrawy M., Sandalio L.M., Dietz K.J., Gonzalez M. & Cejudo F.J. (2010) Functional analysis of the pathways for 2-Cys peroxiredoxin reduction in *Arabidopsis thaliana* chloroplasts. *J Exp Bot*. 2010:61(14):4043-54.

https://doi.org/10.1093/jxb/erq218.4043-4054

Rao Y, Peng T, Xue S. Mechanisms of plant saline-alkaline tolerance. *J Plant Physiol*. 2023:281:153916. https://doi: 10.1016/j.jplph.2023.153916

Rey P, Bécuwe N, Barrault MB, Rumeau D, Havaux M, Biteau B, Toledano MB. The *Arabidopsis thaliana* sulfiredoxin is a plastidic cysteine-sulfinic acid reductase involved in the photooxidative stress response. *Plant J*. 2007:49(3):505-514. https://doi.org/10.1111/j.1365-313X.2006.02969.x

Rey P, Cuiné S, Eymery F, Garin J, Court M, Jacquot JP, Rouhier N, Broin M. Analysis of the proteins targeted by CDSP32, a plastidic thioredoxin participating in oxidative stress responses. *Plant J*. 2005:41(1):31-42. https://doi.org/10.1111/j.1365-313X.2004.02271.x

Rey P, Pruvot G, Becuwe N, Eymery F, Rumeau D, Peltier G. A novel thioredoxin-like protein located in the chloroplast is induced by water deficit in *Solanum tuberosum* L. plants. *Plant J.* 1998:13(1):97-107. https://doi.org/10.1046/j.1365-313x.1998.00015.x

Rey P, Tarrago L. Physiological roles of plant methionine sulfoxide reductases in redox homeostasis and signaling. *Antioxidants (Basel).* 2018:7(9):114. https://doi.org/10.3390/antiox7090114

Rhee SG, Woo HA. Multiple functions of peroxiredoxins: peroxidases, sensors and regulators of the intracellular messenger H_2O_2 and protein chaperones. *Antioxid Redox Signal*. 2011:15(3):781-794. https://doi.org/10.1089/ars.2010.3393

Richter AS, Pérez-Ruiz JM, Cejudo FJ, Grimm B. Redox-control of chlorophyll biosynthesis mainly depends on thioredoxins. *FEBS Lett*. 2018:592(18):3111-3115. https://doi.org/10.1002/1873-3468.13216

Rouhier N, Lemaire SD, Jacquot JP.The role of glutathione in photosynthetic organisms: emerging functions for glutaredoxins and glutathionylation. *Annu Rev Plant Biol*. 2008:59:143-66. https://doi.org/10.1146/annurev.arplant.59.032607.092811

Rumeau D, Peltier G, Cournac L. Chlororespiration and cyclic electron flow around PSI during photosynthesis and plant stress response. *Plant Cell Environ*. 2007:30(9):1041-1051. https://doi.org/10.1111/j.1365-3040.2007.01675.x

Schürmann P, Buchanan BB. The ferredoxin/thioredoxin system of oxygenic photosynthesis. *Antioxid Redox Signal*. 2008:10(7):1235-74. https://doi.org/10.1089/ars.2007.1931

Sekiguchi T, Yoshida K, Okegawa Y, Motohashi K, Wakabayashi KI, Hisabori T. Chloroplast ATP synthase is reduced by both f-type and m-type thioredoxins. *Biochim Biophys Acta Bioenerg*. 2020:1861(11):148261. https://doi.org/10.1016/j.bbabio.2020.148261

Serrato AJ, Pérez-Ruiz JM, Spínola MC, Cejudo FJ. A novel NADPH thioredoxin reductase, localized in the chloroplast, which deficiency causes hypersensitivity to abiotic stress in *Arabidopsis thaliana*. *J Biol Chem.* 2004:279(42):43821-43827. https://doi.org/10.1074/jbc.M404696200

Serrato AJ, Rojas-González JA, Torres-Romero D, Vargas P, Mérida Á, Sahrawy M. Thioredoxins m are major players in the multifaceted light-adaptive response in *Arabidopsis thaliana*. *Plant J*. 2021:108(1):120-133.
https://doi.org/10.1111/tpj.15429

Stenbaek A, Hansson A, Wulff RP, Hansson M, Dietz KJ, Jensen PE. NADPH-dependent thioredoxin reductase and 2-Cys peroxiredoxins are needed for the protection of Mg-protoporphyrin monomethyl ester cyclase. *FEBS Lett*. 2008:582(18):2773-8.
https://doi.org/10.1016/j.febslet.2008.07.006

Sun X, Sun M, Jia B, Qin Z, Yang K, Chen C, Yu Q, Zhu Y. A *Glycine soja* methionine sulfoxide reductase B5a interacts with the $Ca^{(2+)}$ /CAM-binding kinase GsCBRLK and activates ROS signaling under carbonate alkaline stress. *Plant J*. 2016:86(6):514-29.
https://doi.org/10.1111/tpj.13187

Sun H, Zhao W, Liu H, Su C, Qian Y, Jiao F. MaCDSP32 from mulberry enhances resilience post-drought by regulating antioxidant activity and the osmotic content in transgenic tobacco. *Front Plant Sci*. 2020:11:419.
https://doi.org/10.3389/fpls.2020.00419

Sweat TA, Wolpert TJ. Thioredoxin h5 is required for victorin sensitivity mediated by a CC-NBS-LRR gene in Arabidopsis. *Plant Cell*. 2007:19(2):673-687.
https://doi.org/10.1105/tpc.106.047563

Tada Y, Spoel SH, Pajerowska-Mukhtar K, Mou Z, Song J, Wang C, Zuo J, Dong X. Plant immunity requires conformational changes of NPR1 via S-nitrosylation and thioredoxins. *Science*. 2008:321(5891):952-956.
https://doi.org/10.1126/science.1156970

Tarrago L, Laugier E, Rey P. Protein-repairing methionine sulfoxide reductases in photosynthetic organisms: gene organization, reduction mechanisms, and physiological roles. *Mol Plant*. 2009:2(2):202-217.
https://doi.org/10.1093/mp/ssn06

Tarrago L, Laugier E, Zaffagnini M, Marchand CH, Le Maréchal P, Lemaire SD, Rey P. Plant thioredoxin CDSP32 regenerates 1-cys methionine sulfoxide reductase B activity through the direct reduction of sulfenic acid. *J Biol Chem*. 2010:285(20):14964-14972.
https://doi.org/10.1074/jbc.M110.108373

Vieira Dos Santos C, Cuiné S, Rouhier N, Rey P. The Arabidopsis plastidic methionine sulfoxide reductase B proteins. Sequence and activity characteristics, comparison of the expression with plastidic methionine sulfoxide reductase A, and induction by photooxidative stress. *Plant Physiol*. 2005:138(2):909-922.
https://doi.org/10.1104/pp.105.062430

Vieira Dos Santos C, Laugier E, Tarrago L, Massot V, Issakidis-Bourguet E, Rouhier N, Rey P. Specificity of thioredoxins and glutaredoxins as electron donors to two distinct classes of Arabidopsis plastidial methionine sulfoxide reductases B. *FEBS Lett*. 2007:581(23):4371-6.
https://doi.org/10.1016/j.febslet.2007.07.081

Vieira Dos Santos C, Rey P. Plant thioredoxins are key actors in the oxidative stress response. *Trends Plant Sci*. 2006:11(7):329-334.
https://doi.org/10.1016/j.tplants.2006.05.005

Viola S, Bailleul B, Yu J, Nixon P, Sellés J, Joliot P, Wollman FA. Probing the electric field across thylakoid membranes in cyanobacteria. *Proc Natl Acad Sci USA.* 2019:116(43):21900-21906. https://doi.org/10.1073/pnas.1913099116

Vogelsang L, Dietz KJ. Regulatory thiol oxidation in chloroplast metabolism, oxidative stress response and environmental signaling in plants. *Biochem J*. 2020:477(10):1865-1878. https://doi.org/10.1042/BCJ20190124

Wang P, Liu J, Liu B, Feng D, Da Q, Wang P, Shu S, Su J, Zhang Y, Wang J, Wang HB. Evidence for a role of chloroplastic m-type thioredoxins in the biogenesis of photosystem II in Arabidopsis. *Plant Physiol.* 2013:163(4):1710-28. https://doi.org/10.1104/pp.113.228353

Wang J, Song J, Qi H, Zhang H, Wang L, Zhang H, Cui C, Ji G, Muhammad S, Sun G, Xu Z, Zhang H. Overexpression of 2-Cys Peroxiredoxin alleviates the NaHCO3 stress-induced photoinhibition and reactive oxygen species damage of tobacco. *Plant Physiol Biochem*. 2023:201:107876. https://doi.org/10.1016/j.plaphy.2023.107876

Wirtz W, Stitt M, Heldt HW, Light activation of calvin cycle enzymes as measured in pea leaves, *FEBS Letters* 1982:142, 223–226. https://doi.org/10.1016/0014-5793(82)80139-7.

Yang Y, Sulpice R, Himmelbach A, Meinhard M, Christmann A, Grill E. 2006. Fibrillin expression is regulated by abscisic acid response regulators and is involved in abscisic acid-mediated photoprotection. *Proc Natl Acad Sci USA.* 2006:103(15):6061-6066. https://doi.org/10.1073/pnas.0501720103

Yoshida K, Hara A, Sugiura K, Fukaya Y, Hisabori T. Thioredoxin-like2/2-Cys peroxiredoxin redox cascade supports oxidative thiol modulation in chloroplasts. *Proc Natl Acad Sci USA.* 2018:115(35):E8296-E8304. https://doi.org/10.1073/pnas.1808284115

Yoshida K, Matsuoka Y, Hara S, Konno H, Hisabori T. Distinct redox behaviors of chloroplast thiol enzymes and their relationships with photosynthetic electron transport in *Arabidopsis thaliana*. *Plant Cell Physiol*. 2014:55(8):1415-25. https://doi.org/10.1093/pcp/pcu066

Yoshida K, Yokochi Y, Tanaka K, Hisabori T. The ferredoxin/thioredoxin pathway constitutes an indispensable redox-signaling cascade for light-dependent reduction of chloroplast stromal proteins. *J Biol Chem*. 2022:298(12):102650. https://doi.org/10.1016/j.jbc.2022.102650

Zhang H, Liu X, Zhang H, Wang Y, Li T, Che Y, Wang J, Guo D, Sun G, Li X. Thioredoxin-like protein CDSP32 alleviates Cd-induced photosynthetic inhibition in tobacco leaves by regulating cyclic electron flow and excess energy dissipation. *Plant Physiol Biochem*. 2021:167:831-839. https://doi.org/10.1016/j.plaphy.2021.09.016

Zhang H, Xu Z, Huo Y, Guo K, Wang Y, He G, Sun H, Li M, Li X, Xu N, Sun G. Overexpression of Trx CDSP32 gene promotes chlorophyll synthesis and photosynthetic electron transfer and alleviates cadmium-induced photoinhibition of PSII and PSI in tobacco leaves. *J Hazard Mater*. 2020 :398:122899. https://doi.org/10.1016/j.jhazmat.2020.122899

Zhang CJ, Zhao BC, Ge WN, Zhang YF, Song Y, Sun DY, Guo Y. An apoplastic h-type thioredoxin is involved in the stress response through regulation of the apoplastic reactive oxygen species in rice. *Plant Physiol*. 2011:157(4):1884-1899. https://doi.org/10.1104/pp.111.182808

Zimmer D, Swart C, Graf A, Arrivault S, Tillich M, Proost S, Nikoloski Z, Stitt M, Bock R, Mühlhaus T, Boulouis A. Topology of the redox network during induction of photosynthesis as revealed by time-resolved proteomics in tobacco. *Sci Adv*. 2021:7(51):eabi8307.
https://doi.org/10.1126/sciadv.abi8307

Figure legends

Figure 1. Growth of potato plants modified in *CDSP32* expression upon standard or high salinity conditions. A. Three-week old plants grown on soil in a phytotron under standard watering conditions. **B.** Three-week old WT plants watered with standard nutritive solution or solutions containing 0.125 M NaCl or 0.1 M $NaHCO_3$. Arrows indicate leaves at similar developmental stages, smaller in plants treated with NaCl than in those treated with $NaHCO_3$. Histogram representations of the chlorophyll content of young expanded leaves from the upper crown of 24-day old plants grown in standard conditions (**C**), watered with solutions containing 0.125 M NaCl (**D**) or 0.1 M $NaHCO_3$ (**E**). WT, wild type; D4, line co-suppressed for CDSP32; D10, line overexpressing CDSP32; DM19, line overexpressing CDSP32 active site mutant. Chlorophyll data are means ± SD from 22 (NaCl) to 35 (standard and $NaHCO_3$) independent measurements. ** and ***, significantly different from the WT value with $P < 0.01$ and $P < 0.001$, respectively (t-test).

Figure 2. Abundance of CDSP32 and various CDSP32-related plastidial thiol reductases in potato plants modified in *CDSP32* expression grown in standard conditions or exposed to high salinity. A. Western blot analysis of the abundance of CDSP32, 2-Cys PRX, overoxidized 2-CysPRX (2-Cys PRX-Ox), PRXQ, NTRC, MSRB1 and MSRA4 in plants grown in standard conditions or exposed to high salinity treatments, 0.125 M NaCl or 0.1 M $NaHCO_3$, n.s., non specific. **B.** Histogram representation showing the abundance of 2-Cys PRX-Ox, MSRB1 and MSRA4 in plants exposed to $NaHCO_3$. Data are means ± S.D. of four values originating from independent experiments. *, * and ***, significantly different from the WT value with $P < 0.05$, $P < 0.01$ and $P < 0.001$, respectively (t-test). WT, wild type; D4, line co-suppressed for CDSP32; D10, line overexpressing CDSP32; DM19, line overexpressing CDSP32 active site mutant.

Figure 3. Abundance of photosynthetic and photoprotective components in potato plants modified in *CDSP32* expression grown in standard conditions or exposed to high salinity. A. Western blot analysis of the abundance of RubisCO large subunit, PRK, LHCB1, LHCB2, LHCA1, PsbO, PsbA, NDH-H, PGR-L1, ATP-synthase γ subunit, PSBS and FBN/CDSP34 in plants grown in standard conditions or exposed to high salinity treatments, 0.125 M NaCl or 0.1 M $NaHCO_3$. **B.** Histogram representation showing the abundance of PsbO, PsbA and ATP-synthase γ subunit

in plants grown in standard conditions or exposed to high salinity treatments. Data are means ± S.D. of three or four values originating from independent experiments. * and **, significantly different from the WT value with $P < 0.05$ and $P < 0.01$, respectively (t-test). WT, wild type; D4, line co-suppressed for CDSP32; D10, line overexpressing CDSP32; DM19, line overexpressing CDSP32 active site mutant.

Figure 4. Chlorophyll fluorescence parameters in medium-low light. A. Fluorescence induction curves recorded by applying to dark-adapted leaf fragments a multi-turnover saturating pulse followed by 4 minutes of actinic illumination at 80 µmol photons m^{-2} s^{-1} with superimposed saturating pulses. All curves are normalised on Fm-Fo. The red and black arrows indicate the onset (time 0) and offset of the actinic illumination. The means ± S.D. of 3 biological replicates per genotype are shown. The first 4.5 seconds from actinic light onset of the curves are shown with an expanded time scale in panel **B**, to better display the increased transient fluorescence in D4. **C**, **D** and **E.** Maximal PSII quantum yield (Fv/Fm), and PSII yield (Φ_{PSII}) after 4 s and 216 s of actinic illumination, respectively, calculated from the curves in (A). All values represent the means ± S.D. of 3 biological replicates and are reported in Table S2. The Φ_{PSII} 4 s in D4 is significantly lower than in the other genotypes (t-test, ** $P \leq 0.01$, *** $P \leq 0.001$).

Figure 5. Redox-dependent regulation of the chloroplast ATP-synthase activity measured by ECS. A. Representative flash-dependent ECS curves recorded in dark-adapted leaves (closed symbol, solid line), or 2 minutes after a train of 100 (open symbol, solid line) or 300 (closed symbol, dashed line) pre-flashes. **B.** Loss in amplitude of the slow ECS decay phase induced by a variable number of pre-flashes applied to dark-adapted leaves ($-A_n/A_{Dark}$), plotted in function of the number of charge separations PSII+PSI^{-1} generated by the pre-flashes (means ± S.D. of 3 biological replicates for WT, D4 and D10, 5 replicates for DM19). The black and red solid lines represent the Hill fit of the WT and D4 datasets, respectively, and the vertical dashed lines indicate the number of charge separations required to achieve a 50% acceleration of the slow ECS decay phase in the two samples. This number is significantly higher in D4 (t-test, ** $P \leq 0.01$). The fits of the D10 and DM19 datasets are shown in Fig. S6A and B, all fit results are reported in Table S4. **C.** Representative flash-dependent ECS curves recorded in dark-adapted leaves (closed symbol, solid line), or 2 minutes (closed symbol, dashed line) or 8 minutes (open symbol, solid line) after a train of 300 pre-flashes. **D.** Recovery in amplitude of the slow ECS decay phase during a variable dark incubation time after a train of 300 pre-flashes applied to dark-adapted leaves (A_t/A_{Dark}), plotted in function of the dark incubation time (means ± S.D. of 4 biological replicates per genotype). The black and red solid lines represent the Hill fit of the WT and D4 datasets, respectively, and the vertical dashed lines indicate the time of dark incubation required to achieve a 50% recovery of the slow ECS decay phase in the two samples. This time is significantly shorter in D4 (t-test, **** $P \leq 0.0001$).

The fits of the D10 and DM19 datasets are shown in Fig. S6C and D, all fit results are reported in Table S5.

Figure 6. AlphaFold2 structure of *S. tuberosum* CDSP32 (top) and TRX f (bottom). A. The 3D structures are colored according to secondary structure elements (α-helices in pink and β-strands in teal blue). CDSP32 presents two TRX-fold domains (D1 and D2) in tandem, and TRX f a single TRX-fold domain. The Cys residues of the active motif and the Ser residues of the corresponding motif in CDSP32 TRX_D1 are shown in blue. **B.** Surface representation with the same orientation as in **A** displaying atoms colored-coded according to the surface electrostatic potential from red (negative) to blue (positive). Different electrostatic properties are observed between CDSP32 and TRX f in the region surrounding the two redox-active Cys indicated by the yellow circle.

Figure 7. ***S. tuberosum* CDSP32 in complex with ATP synthase γ subunit. A.** AlphaFold2 3D structure of *S. tuberosum* ATP-synthase γ subunit alone showing the L-shaped structure (yellow) containing the redox loop and the β-hairpin. **B.** Complex between CDSP32 and ATP synthase γ subunit generated by AlphaFold2 showing a close proximity between the γ subunit redox loop and the CDSP32 redox active motif, with a close proximity (4Å) of the two catalytic Cys residues of each partner. Superposition of the *S. tuberosum* CDSP32-ATP synthase γ subunit complex onto the spinach ATP-synthase (PDB 6FKF) is shown aside.

Figure 8. Presence of the CDSP32 TRX and of the redox loop in the ATP-synthase γ subunit among photosynthetic organisms. CDSP32 and ATP-synthase γ subunit sequences were analyzed from several species of each main representative group of photosynthetic organisms. The typical CDSP32 19-residue motif surrounding the active site and the redox loop in ATP-synthase γ subunit are shown and Cys residues are underlined. Species: St, *Solanum tuberosum*; Ta, *Triticum aestivum*; Am, *Amborella trichopoda*; Ps, *Picea sitchensis*; Sm, *Selaginella moellendorffii*; Mp, *Marchantia polymorpha*; Cb, *Chara braunii*; Cr, *Chlamydomonas reinhardtii*; Cc, *Chondrus crispus*; Pt, *Phaeodactylum tricornutum;* Eh, *Emiliania huxleyi*; Nc, *Nostoc commune*. Species and accession numbers for CDSP32 : St, NP_001305492.1; Ta, XP_044421501.1; Am, XP_006828837.1; Ps, ABK25354.1; Sm, XP_002989497.2; Mp, PTQ43510.1; Cb, CBR_g26413; Cr, CHLRE_14g624201v5. Species and accession numbers for ATP-synthase γ subunit : St, XP_006348117.1; Ta, XP_044323458.1; Am, XP_006855900.1; Ps, ABK26845.1; Sm, XP_002960916.2; Mp, PTQ27329.1; Cb, GBG67951.1; Cr, XP_001696335.1; Cc, XP_005710884.1; Pt, AAO43198.1; Eh, XP_005761783.1; Nc, WP_196527105.1. ---, absence of *CDSP32* gene or of redox loop in γ subunit.

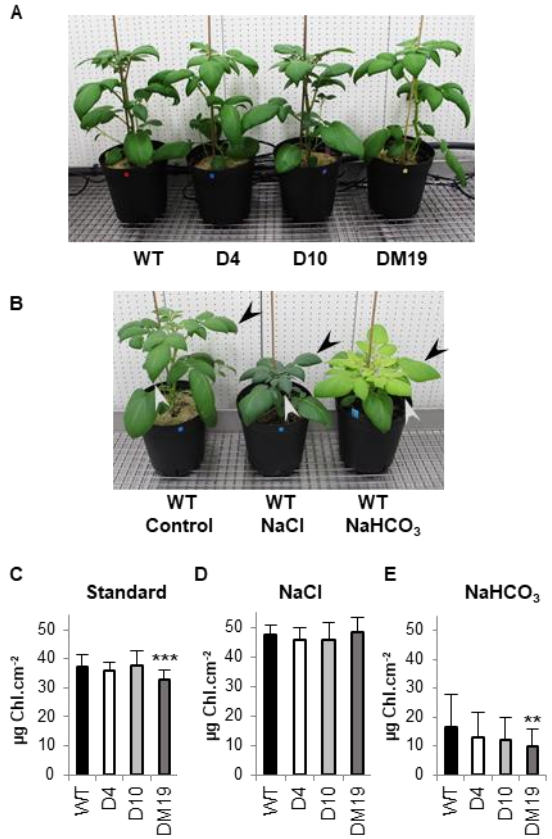

Figure 1. Growth of potato plants modified in *CDSP32* expression upon standard or high salinity conditions. A. Three-week old plants grown on soil in a phytotron under standard watering conditions. **B.** Three-week old WT plants watered with standard nutritive solution or solutions containing 0.125 M NaCl or 0.1 M $NaHCO_3$. Arrows indicate leaves at similar developmental stages, smaller in plants treated with NaCl than in those treated with $NaHCO_3$. Histogram representations of the chlorophyll content of young expanded leaves from the upper crown of 24-day old plants grown in standard conditions (**C**), watered with solutions containing 0.125 M NaCl (**D**) or 0.1 M $NaHCO_3$ (**E**). WT, wild type; D4, line co-suppressed for CDSP32; D10, line overexpressing CDSP32; DM19, line overexpressing CDSP32 active site mutant. Chlorophyll data are means ± SD from 22 (NaCl) to 35 (standard and $NaHCO_3$) independent measurements. ** and ***, significantly different from the WT value with $P < 0.01$ and $P < 0.001$, respectively (t-test).

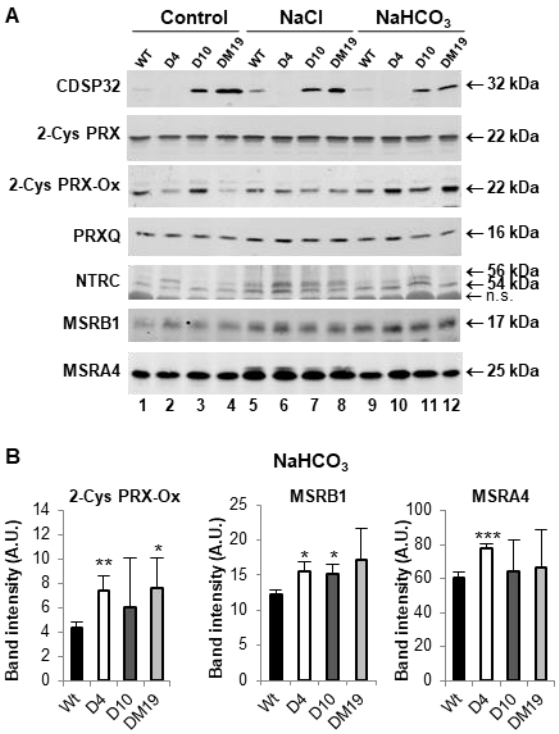

Figure 2. Abundance of CDSP32 and various CDSP32-related plastidial thiol reductases in potato plants modified in *CDSP32* expression grown in standard conditions or exposed to high salinity. **A.** Western blot analysis of the abundance of CDSP32, 2-Cys PRX, overoxidized 2-CysPRX (2-Cys PRX-Ox), PRXQ, NTRC, MSRB1 and MSRA4 in plants grown in standard conditions or exposed to high salinity treatments, 0.125 M NaCl or 0.1 M $NaHCO_3$, n.s., non specific. **B.** Histogram representation showing the abundance of 2-Cys PRX-Ox, MSRB1 and MSRA4 in plants exposed to $NaHCO_3$. Data are means ± S.D. of four values originating from independent experiments. *, * and ***, significantly different from the WT value with $P < 0.05$, $P < 0.01$ and $P < 0.001$, respectively (t-test). WT, wild type; D4, line co-suppressed for CDSP32; D10, line overexpressing CDSP32; DM19, line overexpressing CDSP32 active site mutant.

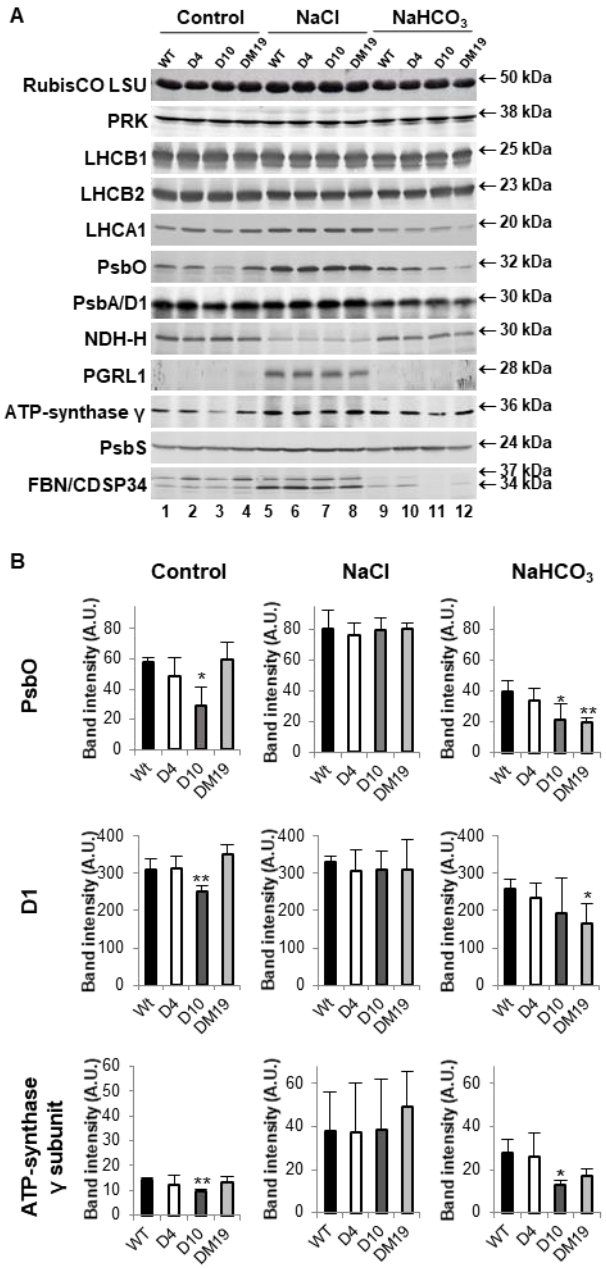

Figure 3. Abundance of photosynthetic and photoprotective components in potato plants modified in *CDSP32* expression grown in standard conditions or exposed to high salinity. A. Western blot analysis of the abundance of RubisCO large subunit, PRK, LHCB1, LHCB2, LHCA1, PsbO, PsbA, NDH-H, PGR-L1, ATP-synthase γ subunit, PSBS and FBN/CDSP34 in plants grown in standard conditions or exposed to high salinity treatments, 0.125 M NaCl or 0.1 M $NaHCO_3$. **B.** Histogram representation showing the abundance of PsbO, PsbA and ATP-synthase γ subunit in plants grown in standard conditions or exposed to high salinity treatments. Data are means ± S.D. of three or four values originating from independent experiments. * and **, significantly different from the WT value with $P < 0.05$ and $P < 0.01$, respectively (t-test). WT, wild type; D4, line

co-suppressed for CDSP32; D10, line overexpressing CDSP32; DM19, line overexpressing CDSP32 active site mutant.

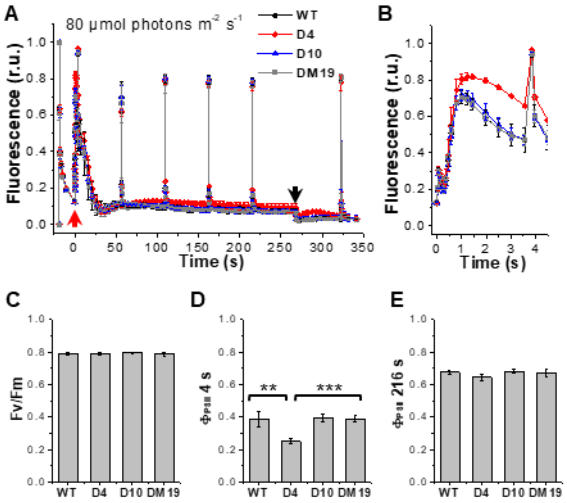

Figure 4. Chlorophyll fluorescence parameters in medium-low light. A. Fluorescence induction curves recorded by applying to dark-adapted leaf fragments a multi-turnover saturating pulse followed by 4 minutes of actinic illumination at 80 µmol photons m^{-2} s^{-1} with superimposed saturating pulses. All curves are normalised on Fm-Fo. The red and black arrows indicate the onset (time 0) and offset of the actinic illumination. The means ± S.D. of 3 biological replicates per genotype are shown. The first 4.5 seconds from actinic light onset of the curves are shown with an expanded time scale in panel **B**, to better display the increased transient fluorescence in D4. **C**, **D** and **E.** Maximal PSII quantum yield (Fv/Fm), and PSII yield (Φ_{PSII}) after 4 s and 216 s of actinic illumination, respectively, calculated from the curves in (A). All values represent the means ± S.D. of 3 biological replicates and are reported in Table S2. The Φ_{PSII} 4 s in D4 is significantly lower than in the other genotypes (t-test, ** $P \leq 0.01$, *** $P \leq 0.001$).

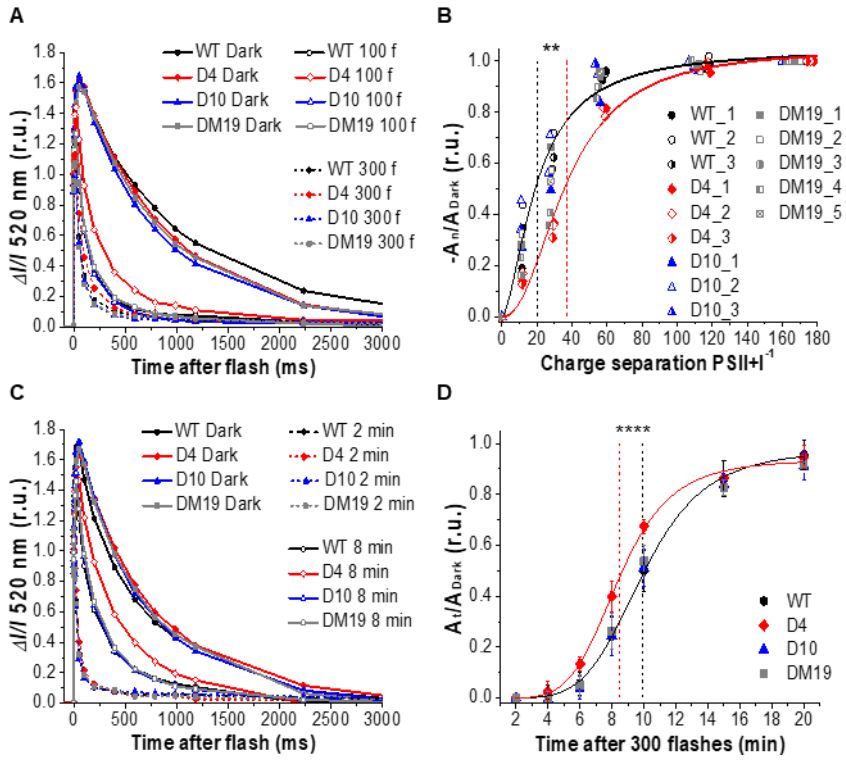

Figure 5. Redox-dependent regulation of the chloroplast ATP-synthase activity measured by ECS. **A.** Representative flash-dependent ECS curves recorded in dark-adapted leaves (closed symbol, solid line), or 2 minutes after a train of 100 (open symbol, solid line) or 300 (closed symbol, dashed line) pre-flashes. **B.** Loss in amplitude of the slow ECS decay phase induced by a variable number of pre-flashes applied to dark-adapted leaves ($-A_n/A_{Dark}$), plotted in function of the number of charge separations PSII+PSI^{-1} generated by the pre-flashes (means ± S.D. of 3 biological replicates for WT, D4 and D10, 5 replicates for DM19). The black and red solid lines represent the Hill fit of the WT and D4 datasets, respectively, and the vertical dashed lines indicate the number of charge separations required to achieve a 50% acceleration of the slow ECS decay phase in the two samples. This number is significantly higher in D4 (t-test, ** $P \leq 0.01$). The fits of the D10 and DM19 datasets are shown in Fig. S6A and B, all fit results are reported in Table S4. **C.** Representative flash-dependent ECS curves recorded in dark-adapted leaves (closed symbol, solid line), or 2 minutes (closed symbol, dashed line) or 8 minutes (open symbol, solid line) after a train of 300 pre-flashes. **D.** Recovery in amplitude of the slow ECS decay phase during a variable dark incubation time after a train of 300 pre-flashes applied to dark-adapted leaves (A_t/A_{Dark}), plotted in function of the dark incubation time (means ± S.D. of 4 biological replicates per genotype). The black and red solid lines represent the Hill fit of the WT and D4 datasets, respectively, and the vertical dashed lines indicate the time of dark incubation required to achieve a 50% recovery of the slow ECS decay phase in the two samples. This time is significantly shorter in D4 (t-test, **** $P \leq 0.0001$). The fits of the D10 and DM19 datasets are shown in Fig. S6C and D, all fit results are reported in Table S5.

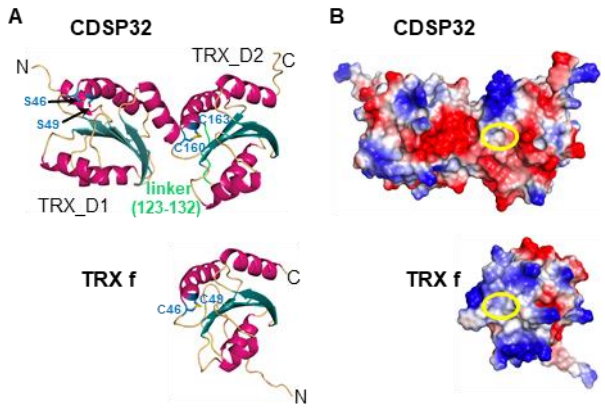

Figure 6. AlphaFold2 structure of *S. tuberosum* CDSP32 (top) and TRX f (bottom). A. The 3D structures are colored according to secondary structure elements (α-helices in pink and β-strands in teal blue). CDSP32 presents two TRX-fold domains (D1 and D2) in tandem, and TRX f a single TRX-fold domain. The Cys residues of the active motif and the Ser residues of the corresponding motif in CDSP32 TRX_D1 are shown in blue. **B.** Surface representation with the same orientation as in **A** displaying atoms colored-coded according to the surface electrostatic potential from red (negative) to blue (positive). Different electrostatic properties are observed between CDSP32 and TRX f in the region surrounding the two redox-active Cys indicated by the yellow circle.

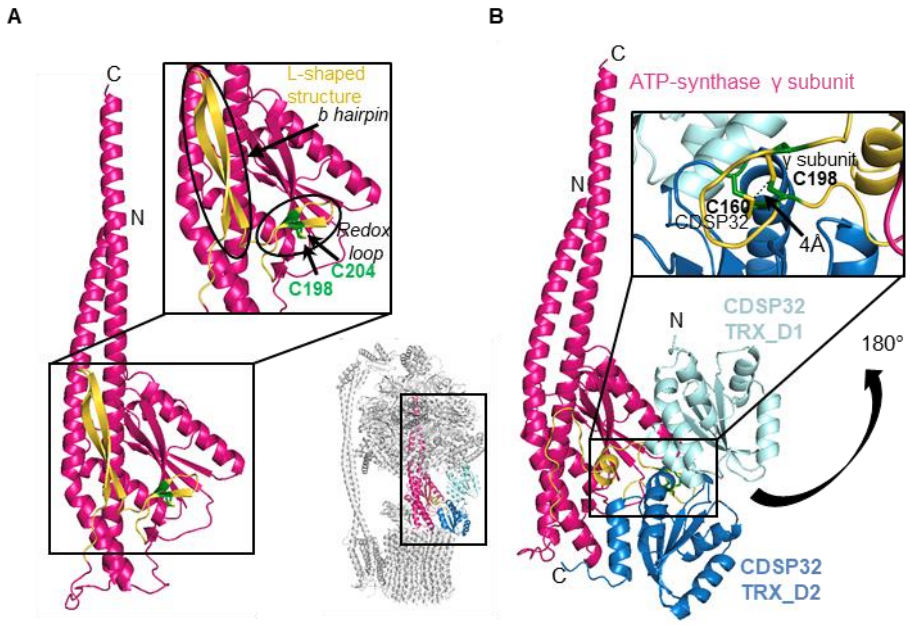

Figure 7. ***S. tuberosum*** **CDSP32 in complex with ATP synthase γ subunit. A.** AlphaFold2 3D structure of *S. tuberosum* ATP-synthase γ subunit alone showing the L-shaped structure (yellow) containing the redox loop and the β-hairpin. **B.** Complex between CDSP32 and ATP synthase γ subunit generated by AlphaFold2 showing a close proximity between the γ subunit redox loop and the CDSP32 redox active motif, with a close proximity (4Å) of the two catalytic Cys residues of each partner. Superposition of the *S. tuberosum* CDSP32-ATP synthase γ subunit complex onto the spinach ATP-synthase (PDB 6FKF) is shown aside.

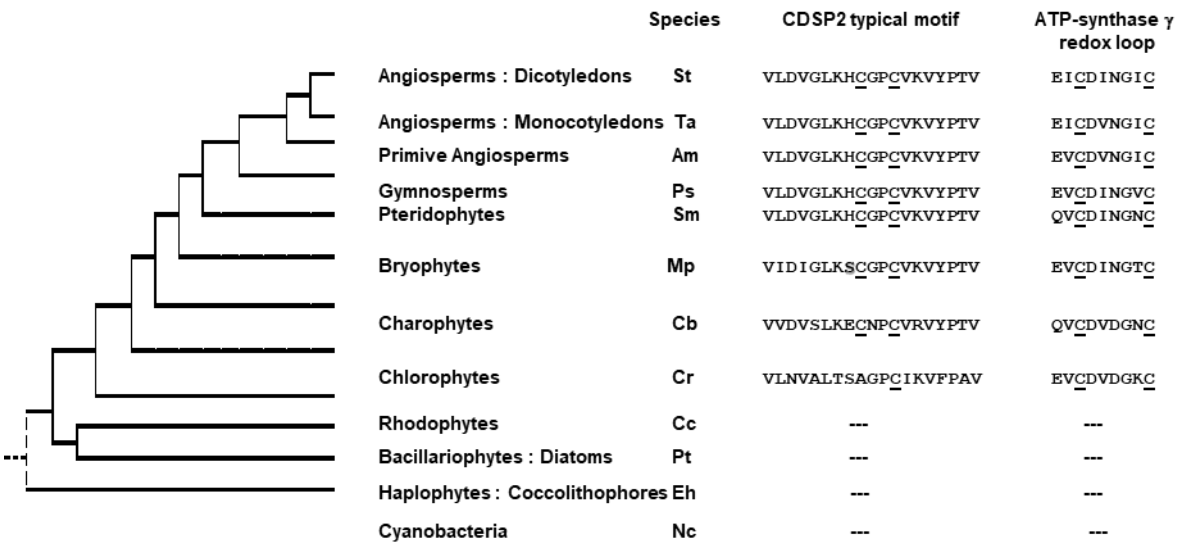

Figure 8. Presence of the CDSP32 TRX and of the redox loop in the ATP-synthase γ subunit among photosynthetic organisms. CDSP32 and ATP-synthase γ subunit sequences were analyzed from several species of each main representative group of photosynthetic organisms. The typical CDSP32 19-residue motif surrounding the active site and the redox loop in ATP-synthase γ subunit are shown and Cys residues are underlined. Species: St, *Solanum tuberosum*; Ta, *Triticum aestivum*; Am, *Amborella trichopoda*; Ps, *Picea sitchensis*; Sm, *Selaginella moellendorffii*; Mp, *Marchantia polymorpha*; Cb, *Chara braunii*; Cr, *Chlamydomonas reinhardtii*; Cc, *Chondrus crispus*; Pt, *Phaeodactylum tricornutum;* Eh, *Emiliania huxleyi*; Nc, *Nostoc commune*. Species and accession numbers for CDSP32 : St, NP_001305492.1; Ta, XP_044421501.1; Am, XP_006828837.1; Ps, ABK25354.1; Sm, XP_002989497.2; Mp, PTQ43510.1; Cb, CBR_g26413; Cr, CHLRE_14g624201v5. Species and accession numbers for ATP-synthase γ subunit : St, XP_006348117.1; Ta, XP_044323458.1; Am, XP_006855900.1; Ps, ABK26845.1; Sm, XP_002960916.2; Mp, PTQ27329.1; Cb, GBG67951.1; Cr, XP_001696335.1; Cc, XP_005710884.1; Pt, AAO43198.1; Eh, XP_005761783.1; Nc, WP_196527105.1. ---, absence of *CDSP32* gene or of redox loop in γ subunit.